NIRS

HIMAC

NIRS-M-89
HIMAC-001

Heavy Ion Medical Accelerator in Chiba
- A Design Summary and Update -

Division of Accelerator Research

December 1992

National Institute of Radiological Sciences

9-1, Anagawa 4-chome, Inage-ku, Chiba-shi 263 JAPAN

Heavy Ion Medical Accelerator in Chiba
-A Design Summary and Update-

Y.Hirao, H.Ogawa, S.Yamada, Y.Sato, T.Yamada, T.Murakami, A.Kitagawa, K.Sato, A.Itano, M.Kumada, E.Takada, M.Kanazawa, K.Noda, M.Sudou, K.Kawachi, F.Soga, M.Endo, T.Kanai, S.Minohara, H.Koyama-Ito and T.Kohno

Division of Accelerator Research,
National Institute of Radiological Sciences

INTRODUCTION

The HIMAC (Heavy Ion Medical Accelerator in Chiba) construction project has been promoted by NIRS (National Institute of Radiological Sciences) as one of the projects of "Comprehensive 10 year Strategy for Cancer Control" which has been come into operation since 1984 by Japanese government.

Radiation therapy has played an important role in cancer treatment, especially with regard to the conservation of organs and their functions. However, patients have not always been satisfactorily treated by conventional radiation (such as X-rays or cobalt gamma rays) because of poor dose localization and the existence of radio-resistant tumors. Recent emphasis of "Quality of Life" view point calls for further development of radiation therapy.

During the last 17 years, NIRS carried out clinical trials involving fast neutrons and protons in place of the commonly used types of radiation for far advanced and highly incurable cancers. Some of the results have indicated significant improvements in the local control rate for tumors involving selected organs[1,2]. These cases are closely related to the excellent physical dose distribution of protons and higher biological effectiveness of neutrons. Furthermore, based on the prospective results of heavy-ion research work at Lawrence Berkeley Laboratory (LBL)[3] and the recent progress in accelerator technology[4], we believe that heavy-ion beams will become significantly superior even to the most effectively used conventional radiation. This scope has stimulated to realize a dedicated heavy-ion medical accelerator.

HIMAC is the first heavy-ion accelerator dedicated to medicine in the world, and its design parameters are based on the radiological requirements. Required ion species were chosen in the atomic number range between 2 (helium) and 18 (argon), as a result of basic research on relative biological effectiveness and of clinical trials at LBL.

The maximum required range of ions in tissue was determined from clinical experience involving conventional radiation therapy at NIRS; range of 30 cm in soft-tissue is sufficient to irradiate deep-seated tumor. The maximum accelerating energy was determined from the range-energy relationship for silicon, which is one of the most suitable and the heaviest ion for the deep-seated and radio-resistant tumor therapy[5]. It should be 800 MeV/u and this maximum energy could provide the range in tissue considerably greater than 30 cm for ions lighter than silicon.

The dose rate requirement for any ion beam is 5 Gy/min to permit completion of one fractional treatment within one minute. The beam intensities for various ion species were estimated from the required dose rate.

The maximum treatment field size of the beam was also selected based on clinical experience at NIRS; most treatments are satisfactory with a maximum field size 22 cm in diameter. The capability to employ both vertical and horizontal beams is essential for

heavy-ion treatment with a highly controlled dose distribution. These medical requirements are summarized in Table 1.

In order to choose an appropriate accelerator system, the most fundamental criteria are the accelerating ion species and the energy range; and they are derived from the medical requirements above. To satisfy these requirements, a synchrotron is the most suitable choice for the main accelerator of this facility. However, since a synchrotron only provides a pulsed beam with a period of a few seconds, it is necessary to prescribe that the time structure of the beam have a long and a flat top intensity in one pulse for precise control of the dose delivered. The specifications are listed in Table 2 as duty factor and repetition rate. The most suitable accelerator complex for the facility was determined by taking into account these specifications and currently existing reliable accelerator technology as well as cost performance.

Figure 1 shows a cross-sectional bird's-eye view of the total layout of the HIMAC facility. It consists of two types of ion sources, an RFQ and an Alvarez linacs, dual synchrotron rings, high energy beam transport lines, and irradiation facilities for treatment and experiments. This report mainly describes the outline of the structure and performance of each HIMAC subsystem.

Table 1. Medical requirements for HIMAC.

Particle Species	He to Ar
Penetrating Range	30 cm in tissue
Dose Rate	5 Gy/min.
Max. Field Size	22 cm ϕ
Beam Direction	Vertical & Horizontal

Table 2. Accelerator specifications.

Ion Species	He to Ar
Maximum energy	800 MeV/u (for ε = 0.5)
Minimum energy	100 MeV/u (for ε = 0.5)
Beam Intensity	2.0 x 10^9 pps/ring (for C)
Duty Factor	20 %/ring
Repetition Rate	0.5 Hz/ring

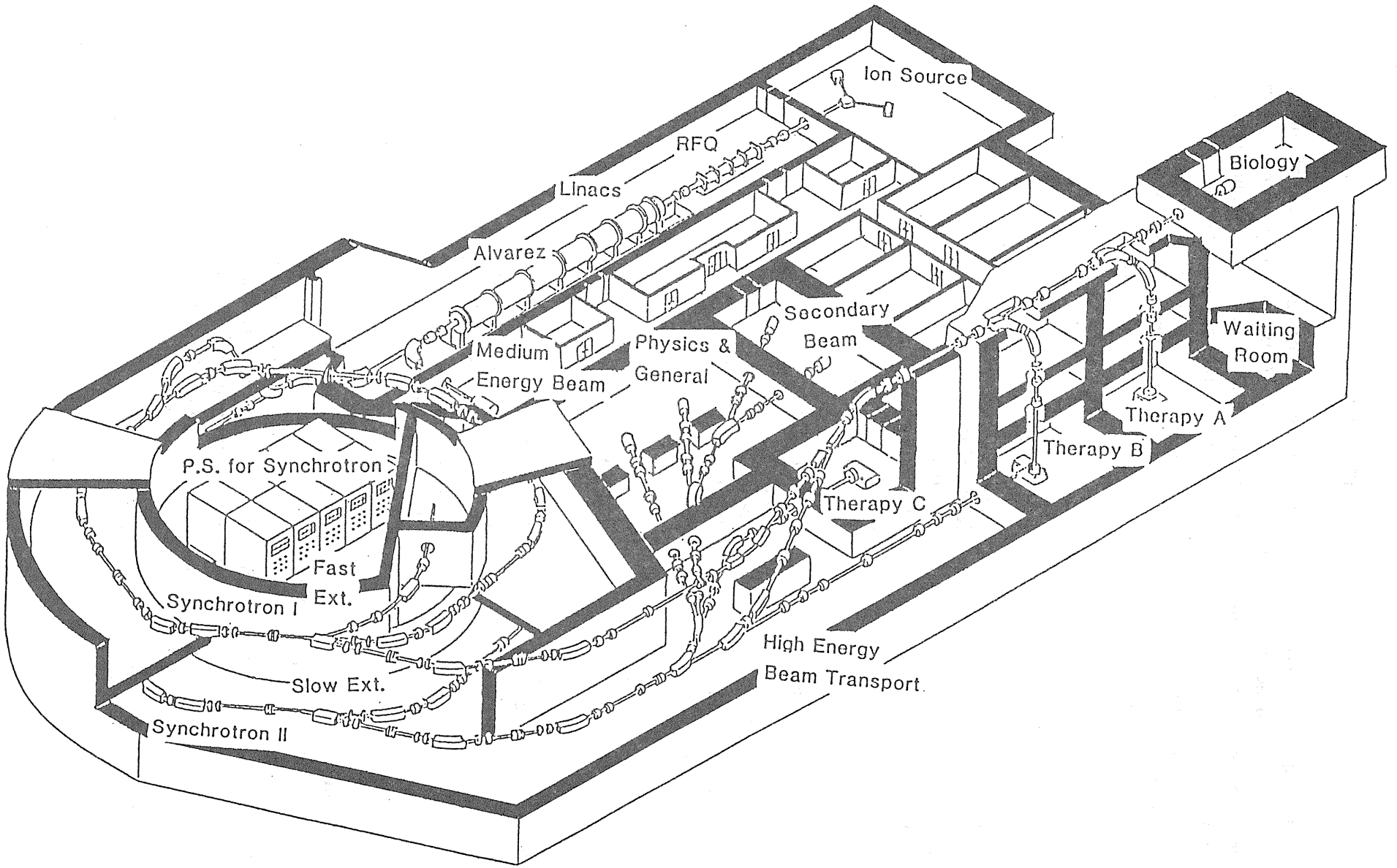

Fig. 1. Bird's eye view of the HIMAC facility.

INJECTOR

The injector system comprises two types of ion sources, an RFQ linac of 100 MHz and three Alvarez type linac tanks with the same frequency[6–9]. A debuncher cavity is installed in a medium energy beam transport (MEBT) line in order to reduce a momentum spread of the output beam. The system has no charge stripper either between or before the linac tanks, except for a stripping foil installed in the MEBT line. The whole linac system can accept heavy ions with a charge–to–mass ratio as small as 1/7. The specifications and a layout of the overall injector system are presented in Table 3 and Fig. 2, respectively.

Table 3. Injector specifications.

Ion species	^{4}He to ^{40}Ar
Charge to mass ratio	≥ 1/7
Ion source type	PIG & ECR
Frequency	100 MHz
Repetition rate	3 Hz Max.
Duty factor	0.3% Max.
Acceptance	0.6π mm·mrad (normalized)
RFQ linac	
Input/Output energy	8 / 800 keV/u
Vane length	7.3 m
Cavity diameter	0.59 m
Max. surface field	205 kV/cm (1.8 Kilpatrick)
Peak rf power	260 kW (70% Q)
Alvarez linac	
Input/Output energy	0.8 / 6.0 MeV/u
Total length	24 m (3 rf cavities)
Cavity diameter	2.20 / 2.18 / 2.16 m
Average axial field	1.8 / 2.2 / 2.2 MV/m
Shunt impedance	31 ~ 46 MΩ/m (effective)
Max. surface field	150 kV/cm (1.3 Kilpatrick)
Peak rf power	840 / 830 / 770 kW (75% Q)
Focusing sequence	FODO (5.1 kG/cm Max.)
Output beam emittance	≤ 1.5 π mm·mrad (normalized)
Momentum spread	≤ ± 1 x 10^{-3}

ION SOURCES

There are two types of ion sources in the injector system in order to keep the reliable and stable operation of the accelerator system; a PIG and an ECR sources. The PIG source is used mainly for the production of light heavy ions whereas the ECR source is expected to improve heavier ion capabilities and is basically maintenance free. Each ion source covers from He to Ar at least. When one source is operating for normal radiotherapy program, the other one is standing by. The injection energy to the linac is 8 keV/u. For this, the sources are put on the high voltage platforms (60 kV at the maximum).

The PIG source is an indirectly heated (hot) cathode type. Due to the application of low temperature ions at the plasma growth[10] and the high electron current density by low gas–pressure[11], peak current of 2 – 3 mA for C^{2+} and Ne^{3+} were obtained under low–duty

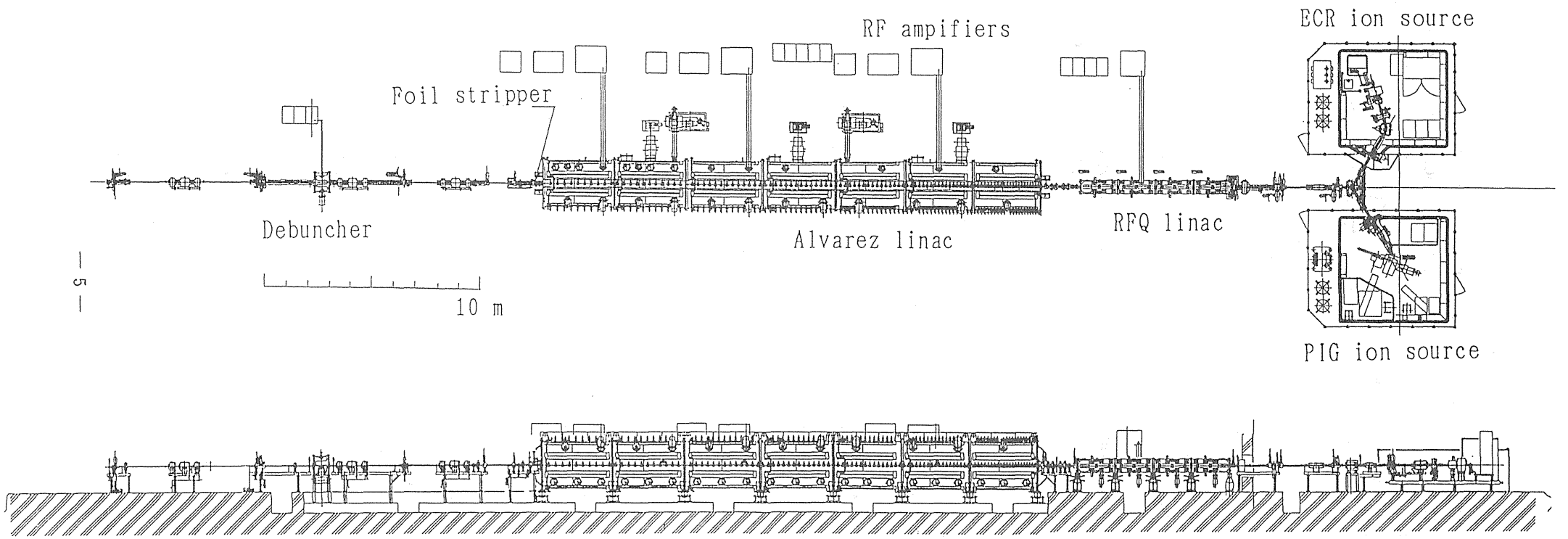

Fig. 2. Layout of injector system.

pulsed operation. Latest performances are listed in Table 4. The emittance is about 250 πmm·mrad both in the x and y directions. The duty factor for the pulsed operation is 4 x 10^{-4} at a repetition rate of 1 Hz (10 Hz at the maximum), which is synchronized to the synchrotron. The peak discharge power is 2 – 3 kW (1 W in the average), and the extraction voltage is 25 kV. The lifetime of the source is determined by that of filament, and is about two weeks[12]. In the long–term stability test of the extracted beam, no adjustment of the source parameters was necessary throughout 24 hours.

The ECR source has a simple single–stage structure[13]. A microwave source of 10 GHz (1.9 kW) is applied for the ECR acceleration. The magnetic field structure for the acceleration and confinement of hot electrons consists of the 10 kG axial field by two solenoids and the 8 kG radial field on the wall of the chamber by a set of permanent sextupole magnets. The bore diameter of the plasma chamber is 70 mm. Recent performance is shown in Fig. 3. At present, several gaseous ions were obtained in the dc operation. When highly charged ions were optimized, a typical gas–flow was about 5 x 10^{-4} Torr·l/sec and the vacuum pressure about 1 x 10^{-6} Torr in the chamber. In the case of pulsed operation, an increase of ion beams is expected by the "afterglow" peak[14].

RFQ

The ions pass through a low energy beam transport (LEBT) line of about 7 m before injection into an RFQ linac. The focusing elements in the LEBT line are einzel lenses, solenoid coils, electrostatic quadrupoles, and bending magnets. The vacuum pressure of the line will be maintained in a range of 10^{-7} Torr with TMP's.

The RFQ linac is a conventional four vane type and separated longitudinally into four tanks. The four vanes are precisely set in each tank independently. A longitudinal and a transverse voltage distributions are tuned with about 40 side tuners within errors of 4.9% and 2.6%, respectively. The tuners are fixed by welding after the voltage tuning. The tank is made of copper plated mild steel, whereas the vanes are solid copper. The rf contact between the vanes and the tank wall is achieved with silver coated stainless steel spring–rings. The entire linac tank is fed with a 300 kW peak rf power through a single loop coupler.

A rather low frequency of 100 MHz is chosen for the RFQ in order to obtain the sufficient focusing strength. A calculated transmission efficiency exceeds 90% for a DC beam with a focusing strength of B = 3.8. The low value of B is adopted because of advantages in getting a high acceleration efficiency. An acceptance of the RFQ linac is 0.6 πmm·mrad normalized (145 πmm·mrad unnormalized).

A number of unit cells in the radial matching section is determined to be 40 so that the convergence angle of the input beam becomes as small as 60 mrad. The parameters of the RFQ are listed in Table 5.

The RFQ linac is followed by an Alvarez type linac (DTL) operated at the same frequency. The transverse phase space matching between these two types of linac is accomplished with a quadrupole magnet quadruplet and a horizontal and a vertical steering magnets in an interlinac transport line (LLBT). The LLBT is about 1.9 m long, and some beam diagnostic apparatus of a Faraday cup, an electrostatic pickup electrode, *etc.* are installed in the relatively long transport line.

A phase spread of the accelerated beam is estimated to be 20° at the output end of the RFQ, and will be increased to 70° during the travel along the LLBT due to a large momentum spread of the beam. A calculation with PARMILA shows that a transmission efficiency through the DTL is not seriously affected by the wide phase spread even for the beam having three times larger longitudinal emittance than an ideally calculated value at the RFQ output. The longitudinal emittance growth in the LLBT, however, tends to introduce an

Table 4. Latest performance (emA) of the low-duty pulsed PIG source in NIRS. The underlined ions (e/m = 1/7) will be usually accelerated in the injector of HIMAC.

Atom	gas-flow (cc/min)	1+	2+	3+	4+	5+	6+	7+	8+
^{4}He	~ 20 (He)	<u>3.5</u>	3.0						
^{12}C	0.6 (CO_2)	1.0	<u>3.5</u>	3.0**	0.6	0.02			
^{14}N	0.6 (N_2)		<u>2.0</u>	2.5	1.2	0.2			
^{16}O	0.6 (CO_2)		2.0	<u>2.3</u>	3.0**	0.3	0.03		
^{20}Ne	1.1 (Ne)		2.0	<u>2.0</u>	0.8	0.4	0.02		
$^{28}Si^{*}$	0.3 (Ar)			0.4	<u>0.6</u>	0.3	0.05	0.01	
^{40}Ar	0.2 (Ar)			1.5	1.9	1.8	<u>0.8</u>	0.4	0.2

*Si ions are produced by sputtering the silicon single crystal with Ar.
**O^{4+} and C^{3+} are mixed each other due to an identical e/m.

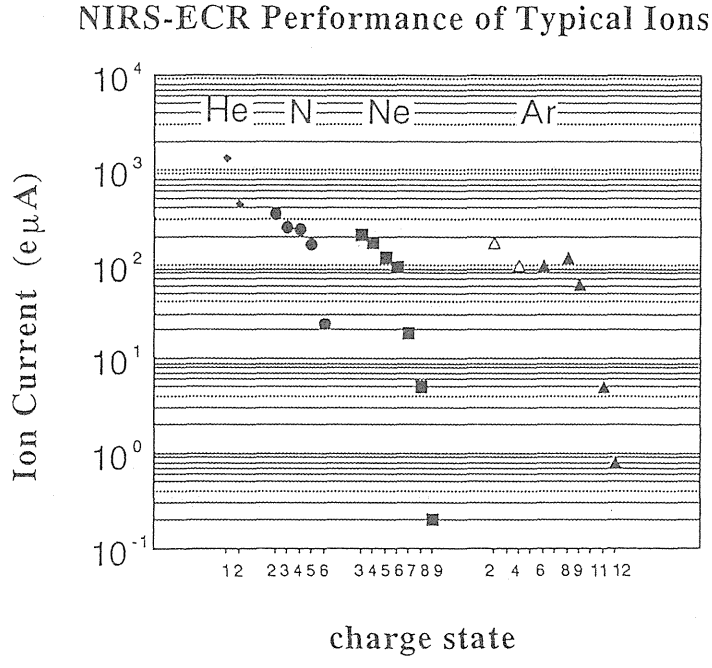

Fig. 3. Performance of the ECR ion source.

unwanted momentum spread at the output end of the DTL. An input value of a macroscopic longitudinal emittance of 5.5 mrad·MeV/u increases to 18 mrad·MeV/u by a factor of 3.3 after acceleration with the DTL.

ALVAREZ LINAC

The Alvarez type linac is separated into three independent rf cavities and each cavity is fed with an rf power of about 1 MW peak. The maximum surface field is chosen to be 150 kV/cm (1.3 Kilpatrick) to realize an average axial field of about 2 MV/m. The linac tank is 24 m long in total, and consists of 106 unit cells. The diameter of the cavity is about 2 m and changes with one tank to the next in order to obtain reasonable values for the transit time factors. A gap to cell length ratio takes a value around 0.22. The major parameters of the Alvarez linac are listed in Table 6. A photograph of an inside view of the first Alvarez tank is given in Fig. 4.

The tanks are made of copper–clad mild steel, and the drift tubes are copper–plated stainless steel. The thicknesses of the clad and plated copper are 8 mm (before machining) and 100 μm, respectively. Each drift tube is supported by horizontal and vertical stems, the diameters of which are 3 and 5 cm, respectively. Every second drift tube is equipped with a quadrupole magnet. The magnets have laminated cores and are excited by pulse power sources with a very low flat–top–duty of 0.3% in order to reduce the heavy thermal loads. Since the transverse emittance of the beam from the RFQ is thoroughly small, a FODO type focusing structure is adopted for the Q–magnets.

The 53 quadrupole magnets in the drift tubes are standardized with four different groups: lengths of the magnets are 70, 90, 135 and 165 mm, and field strengths are 5.1, 4.0, 2.7 and 2.2 kG/cm, respectively. The 47 independent power supplies are prepared for these magnets. An amplitude of vibration of a drift tube, which is caused by a rapid change in the magnetic field of the Q–magnet, is negligible.

The allowable alignment errors for the Q–magnets in the drift tubes are estimated with PARMILA program. The transverse emittance growth is not so serious when the alignment error is $\leq \pm 0.1$ mm in the transverse direction together with the rotation error of $\pm 1°$, the tilt error of $\pm 1°$, and the excitation error of $\pm 0.5\%$. The ellipse parameters in the transverse phase diagram of the accelerated beam are almost kept constant against the error. The center of the ellipse, however, moves around the origin and needs a set of steering magnets in the MEBT line to be matched with the optical axis.

The calculations are also made with the errors in the acceleration field including the field tilt and the phase errors. The phase differences between three tanks affect strongly on the output beam quality when they are greater than $\pm 3°$. The effects of the field tilt, however, are not serious even when the tilt is as high as 10%. An automatic phase controlling system, therefore, is developed to keep the error within $\pm 1°$ with respect to the master oscillator. High power tests using the third DTL cavity show that the system works very stably as expected[9].

A case study for the trouble of a Q–magnet has been done. The transmission efficiency through the linac decreases to 46% when one of the Q–magnets shuts down. An output phase diagram also changes appreciably. The re–tuning of two adjacent Q–magnets (including the change of the polarity), however, recovers the beam characteristics very well when the input beam is properly adjusted.

CHARGE STRIPPER AND DEBUNCHER

At the output end of the Alvarez linac, a 100 $\mu g/cm^2$ carbon stripping foil is installed in order to improve a charge–to–mass ratio for further acceleration. Only one stripping section

Table 5. RFQ linac specifications.

Operation frequency	100 MHz
Input / Output energy	8 / 800 keV/u
Charge to mass ratio	1 / 7
Synchronous phase	−90 ~ −30 deg.
Transmission efficiency	0.92
Number of unit cells	300
Vane length	725 cm
Cavity diameter	59 cm
Characteristic bore radius	0.54 cm
Minimum bore radius	0.29 cm
Maximum modulation	2.5
Focusing strength	3.8
Acceptance	145 πmm·mrad
Normalized acceptance	0.6 πmm·mrad
Intervane voltage	81 kV
Maximum field	205 kV/cm (1.8 Kilpatrick)
Peak rf power	260 kW (70% Q)

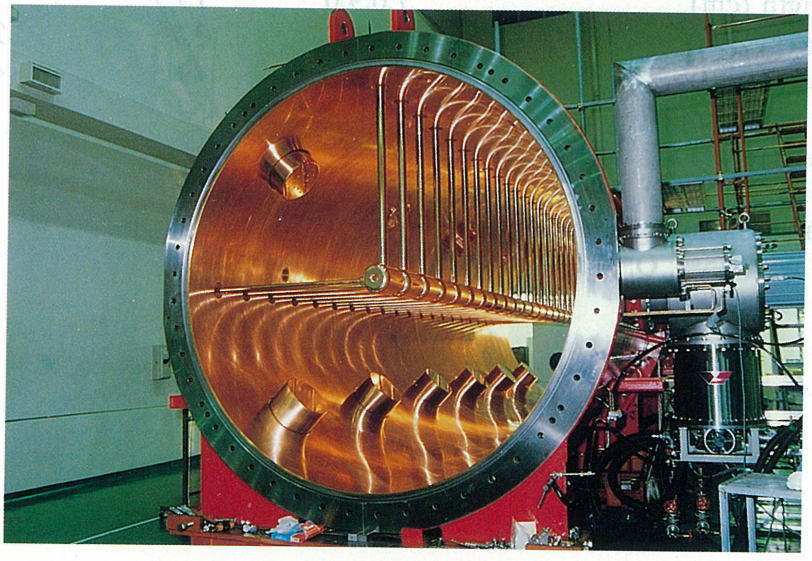

Fig. 4. Photograph of the Alvarez tank

Table 6. Alvarez linac specifications.

	Tank 1	Tank 2	Tank 3
Synchronous phase (deg)	−30		
Ion energy (MeV/u)	0.800 – 2.669	2.669 – 4.385	4.385 – 6.060
velocity (%)	4.127 – 7.526	7.526 – 9.634	9.634 – 11.31
Average axial field (MV/m)	1.81	2.20	2.20
Effective shunt impedance*(MΩ/m)	31.5 – 38.7	41.5 – 42.9	45.2 – 45.6
Transit time factor	0.825 – 0.853	0.869 – 0.867	0.888 – 0.880
Quality factor of cavity*	132,000	141,000	143,000
Tank length (m)	9.768	7.202	6.907
Acceleration rate (MeV/m)	1.34	1.67	1.70
Tank diameter (m)	2.20	2.18	2.16
Drift tube diameter	16.0	16.0	16.0
Drift tube length (cm)	9.85 – 16.45	17.99 – 21.72	22.90 – 25.73
Bore radius (cm)	1.0	1.5	1.5
Nose corner radius (mm)	20	30	30
Unit cell length (cm)	12.45 – 22.47	22.67 – 28.77	28.99 – 33.79
Gap to cell length ratio	0.214 – 0.265	0.210 – 0.242	0.213 – 0.236
Number of unit cells	56	28	22
Stem radius (cm)	5 and 3	5 and 3	5 and 3
Shunt impedance*(MΩ/m)	46.29 – 53.16	54.93 – 57.07	57.38 – 58.92
Required rf power**(kW)	840	830	770
Q–magnet sequence	FODO	FODO	FODO
Q–magnet length (cm)	7.0,9.0	13.5	16.5
Field gradient (kG/cm)	5.1,4.0	2.7	2.2
Phase advance (deg)	42	49	49
Acceptance (πmm·mrad)	67	–	–
Normalized acceptance (πmm·mrad)	2.8	–	–

*Superfish value including stem losses.
** Estimated with 75% Q.

is used at a relatively high ion energy because of the reliability of the system and of future expansion to the acceleration of heavier ions.

A 100 MHz debuncher cavity is introduced in the output beam line to suppress the momentum spread of the accelerated beam. A distance between linac end and the debuncher cavity has been optimized to be about 10 m. A phase spread at the debuncher position is broadened to about ±50° after the long travel along the MEBT line. An rf voltage of 300 kV (for $q/A = 1/4$) rotates the beam bunch in longitudinal phase space, and reduces the energy spread of the linac beam from $\Delta W/W = \pm 1.2\%$ to a satisfactorily good value of ±0.11%. Some kind of tuning error of the Alvarez linac, however, tends to increase the energy spread up to more than ±0.2%. An error of relative phases in the acceleration fields among DTL tanks affects most seriously on the energy spread.

RF SYSTEM

An rf amplifier of the Alvarez linac is designed to deliver more than 1.4 MW and is equipped with a power tube of Siemens' RS 2074 SK. In the two driver stages of the amplifier system, RS 2058 CJ and RS 2032 CL vacuum tubes have been adopted and deliver rf powers of 100 and 5 kW, respectively. Three sets of 1.4 MW amplifiers with a single plate power supply will be used to excite the three Alvarez cavities. The construction of the amplifiers for Alvarez linac are already finished, and the high power tests including the parallel operation of these three amplifiers are also successfully done.

In a 300 kW amplifier for the RFQ linac, the Eimac tubes have been adopted: 4CW 100,000E for the final stage and 4CX20,000C for the driver stage. A 30 kW amplifier for the debuncher cavity is the same as the driver amplifier.

CONTROL SYSTEM

A computer system of the injector consists of three mini-computers: a system control unit (SCU) of μVAX 3500 and two group control units (GCU) of μVAX II. The SCU mainly covers the man-machine interface and controls the injector as a total system, whereas the GCU directly controls a peripheral device through a universal device controller (UDC), which is a 16-bit micro-computer installed within the device.

The SCU is connected to a central computer unit through an ethernet by which other control units for a synchrotron system and a high energy beam transport system etc. communicate with each other. A control computer for medical treatment will also be connected to the network. Another ethernet is used to realize communication between the SCU and the GCUs. The GCU and each UDC are linked with an optical fiber line.

All devices in the injector system, including a timing unit, are controllable from an operator console with four touch panels and three rotary encoders.

RF CHARACTERISTICS OF LINAC TANKS

An inside diameter of the tank was machined within an error of ±0.3 mm. After that, the copper surface was treated with an orbital sander to a surface roughness of 0.4a (1.2s). An alignment accuracy of better than ±0.1 mm has been achieved for the transverse position of a drift tube with an alignment telescope and an optical target inside a bore hole of the tube. The bore hole was machined with an accuracy of ±10 μm after measurements of a center position of the quadrupole field. A longitudinal positioning error of the drift tube was measured to be better than ±0.2 mm.

A resonant frequency of the cavity exists very close to a desired value with calculated positions of the frequency tuner. The frequency is about 1 MHz apart from the nearest neighboring mode of TM_{011} for the DTL no. 3 tank (Q_0 is about 50,000). An unloaded

Q–value, Q_0, of the fundamental TM_{010} mode was measured to be 88,000 for a virgin tank and the value is about 70% of a calculated value including stem losses.

A tilt of the acceleration field was tuned with six side tuners within an error of 2%. The positions of the tuners were fixed after the low power measurements by welding. A small jump (about 2%) in the acceleration field appears at the end of the tank where a unit cell volume is reduced a little bit with a 2.5 cm thick copper wall separating the cavity from the next one.

Field and frequency measurements were carried out in order to obtain dependencies on a longitudinal position and a radius of an end drift tube. All efforts, however, resulted in little effects on the compensation of the field jump at the end cell. The field distribution in the acceleration gaps was also measured with a bead pull method. The results were very well reproduced by the calculated values. The resonant frequency changes with the cavity temperature by 1.2 ~ 1.4 kHz/deg. and the value agrees well with the calculated one.

A full design power was successfully injected into the virgin cavity after conditioning of about one whole day. There was no visible damage to the coupling loop and any other components. A maximum surface field of 150 kV/cm (1.3 Kilpatrick) is stably obtained.

A length of a coaxial line between the amplifier and the cavity is optimized with a trombone tuner so that coupling between the amplifier and the cavity takes its minimum value. A rise time (0 to 90% value) of the field level is about 500 μs without any feed back loop, and about 50% longer than a simply predicted value of 320 μs. The rise time, however, is reduced to about 400 μs with an automatic gain control loop. A flatness better than $\pm 1 \times 10^{-3}$ is obtained in the duration of more than 700 μs for an rf pulse width of 1.2 ms.

Phase stability was measured to be better than ±0.5°/8hr with an automatic phase controller, and well within the acceptable range. After a long run test of 24 hr, the unloaded Q–value of the cavity was improved to 102,000 (79% of SUPERFISH value).

SYNCHROTRON

A main accelerator consists of two synchrotron rings which are followed by independent horizontal and vertical high energy beam transport system[15,16,17]. Two rings are located at lower and upper underground floors with vertical distance 7 m between them. They are operated independently from each other except that the synchrotron magnets of each ring are excited 180° out of phase. A summary of the major parameters of the synchrotron is given in Table 7. Injection beam transport system receives the beam from injector linac and switch it to upper and lower rings alternatively to match the alternative operation of the two rings. Two rings have almost an identical lattice structure. They both have a multiturn injection channel and a slow extraction channel. The output energy of each ring is variable in a wide range from 100 MeV/u to 800 MeV/u. Extraction beam transport line sends the extracted beam to the downstream high energy beam lines. The two-ring structure of the synchrotron makes it possible to supply horizontal and vertical beams with different energies to one treatment room or to two different treatment rooms simultaneously. In future extension, two-stage acceleration of heavier ions will be possible. Electron cooling is very important in the extension to improve the beam quality. It will be also feasible that the lower ring is used as a storage ring, aiming at treatments and diagnosis with radioactive beam and/or single shot beam. In this respect the upper ring is designed to have a fast extraction channel, whereas the lower ring is designed to have a fast injection channel.

Table 7. Summary of major synchrotron parameters.

Maximum rigidity	9.75 Tm
Injection energy	6 MeV/u
Output energy	100 – 800 MeV/u
Maximum intensities for light ions	10^{11} ppp
Repetition rate	0.3 – 1.5 Hz
Injected emittance Hor/Ver	264 / 26.4 πmm-mrad
Momentum spread after rf turned on	±0.7 %
Number of injected turns	40
q/A except Ar^{18+}	0.5
Vacuum	$5x10^{-9}$Torr
Lattice type	FODO
Circumference	129.6 m
Periodicity	6
Cells per period	2
Long/Short straight section length	5.0 / 0.8 m
Dipole field at full rigidity	1.5 T
Quadrupole gradient at full rigidity	7.4 T/m
Betatron tunes Q_H / Q_V	3.75 / 3.25
Natural chromaticity ξ_H/ξ_V	-3.90 / -3.99
Cooling system heat load	5.4 MW

INJECTION BEAM TRANSPORT SYSTEM

The injection beam transport system[18] receives the beam from the linac and switches it to upper and lower synchrotron rings alternatively by using a fast switching magnet. The magnet power supply has 140 msec field rising and falling times. The flat top length of the output current is larger than 3 msec with stability better than $\pm 1 \times 10^{-4}$.

The system is designed such that the Twiss parameters at the entrance of each ring is easily adjustable to match the optical condition of multiturn injection. A beam momentum and a charge to mass ratio of the beam are analyzed by measuring the field strength of the first bending magnet of the transport system by NMR and by using slit system. This facilitates an efficient beam transport and a beam tuning in the ring. A double achromatic condition at the entrance of the ring can be realized by adjusting quadrupole magnets in the system. A gap between a septum and a high voltage electrode of the electrostatic inflector can be reduced and therefore the high voltage value can be reduced.

Acceptance of the transport system is 26.4 πmm-mrad in absolute value both in horizontal and vertical planes. Momentum acceptance $\Delta p/p$ is ± 0.3 %.

RING LAYOUT

Synchrotron ring is of a separated function type with a strong FODO focusing structure. The synchrotron ring consists of 12 dipole magnets, 12 focusing quadrupole magnets and 12 defocusing quadrupole magnets. Super periodicity of the ring is set to 6 for the efficient use of defocusing strength of the defocusing quadrupole in the long straight section at extraction. Designed tunes of the ring are 3.75 (Horizontal) and 3.25 (Vertical). Fig. 5 shows a lattice structure and a lattice function for one period of the lattice. A field monitoring dipole magnet to generate a field clock (B clock) for rf acceleration is located inside the ring.

The two rings have a multiturn injection channel and a slow extraction channel. The upper ring is designed to have a fast extraction channel at the same long straight section as for the slow extraction. The fast beam will be extracted inside the ring. It is also designed that the lower ring has a fast injection channel to receive the fast extraction beam from the upper ring. Extraction and injection processes generate bump orbits partially in the ring. Apparatus located along the bump orbits must have a larger aperture. Apparatus critical in aperture such as rf accelerating cavities and scrapers are located outside the bump orbits. Figure 6 shows a layout of the upper synchrotron ring.

Horizontal closed orbit distortion (COD) is corrected dynamically up to the flat top by 12 horizontal steering magnets. Residual COD after correction is estimated to be 4 mm (3 σ) by Monte Carlo simulation. Spaces for 12 vertical steering magnets are reserved to correct vertical COD in occasional deformation of the building floors in future.

Natural chromaticities of the ring are -3.90 (Horizontal) and -3.99 (Vertical). A set of 6 sextupole magnets is installed for horizontal chromaticity correction. Spaces for another set of 6 sextupole magnets are reserved for vertical chromaticity correction.

A single rf accelerating cavity is installed in the ring for the first construction phase. A space for the second accelerating cavity is reserved.

MULTITURN INJECTION CHANNEL

Multiturn injection scheme is used to inject the beam from the linac into the ring. Designed value of the injecting beam emittance is 1.5 πmm-mrad (normalized). Horizontal ring acceptance is 30 πmm-mrad (normalized), i.e., 264 πmm-mrad in absolute value. The number of the injected turn is 40. The vertical acceptance of the ring is 26.4 πmm-mrad in absolute value.

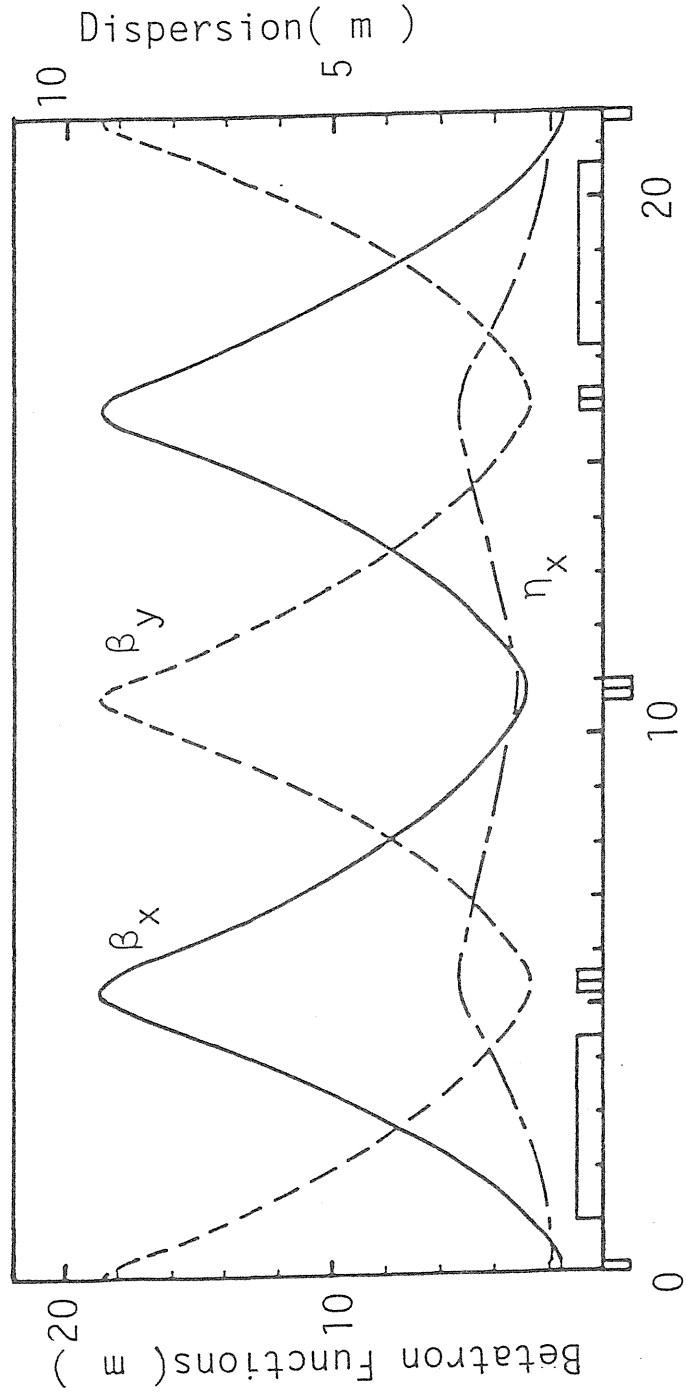

Fig. 5. Betatron and dispersion functions of HIMAC synchrotron lattice.

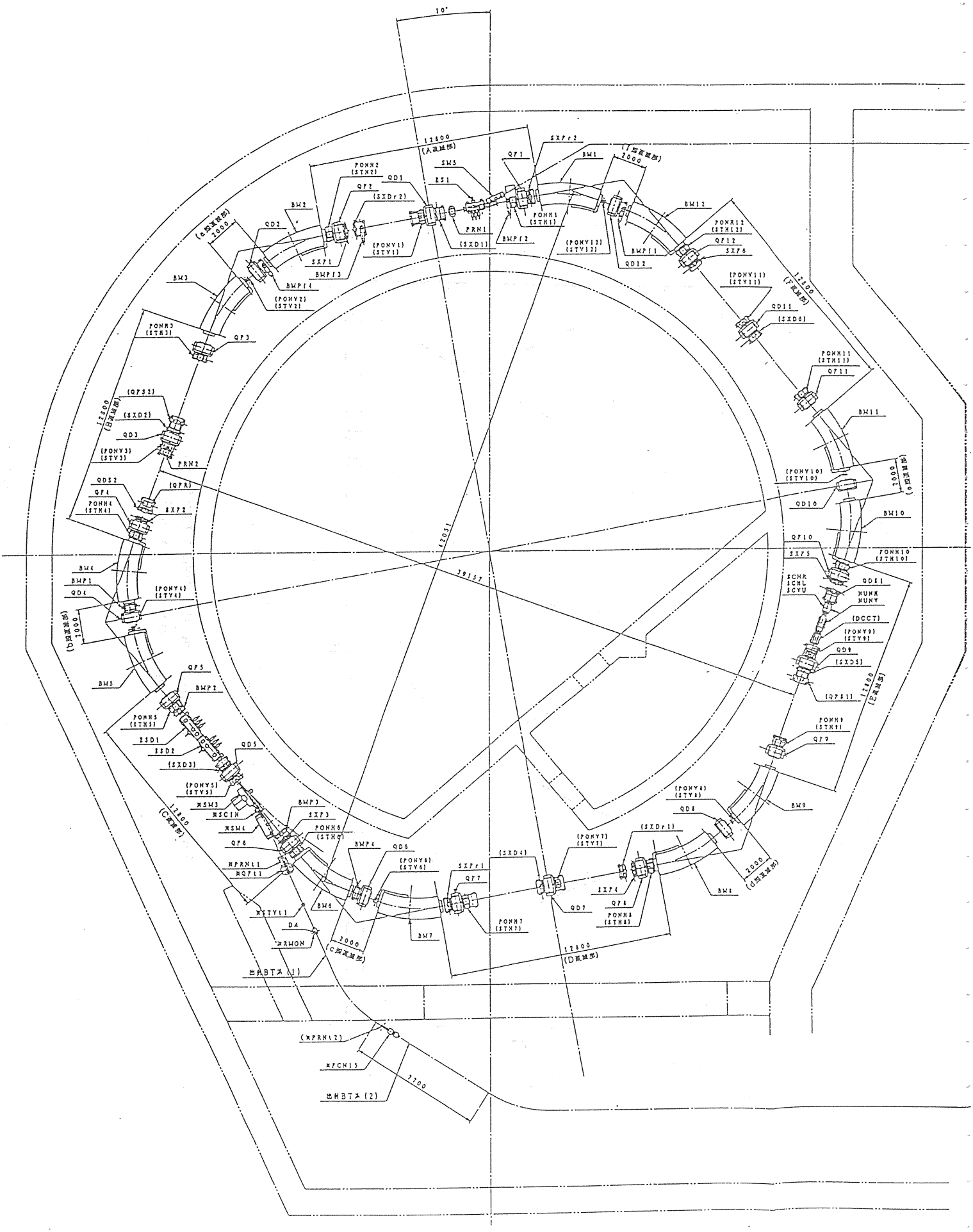

Fig. 6. Layout of the upper synchrotron ring.

A 0.7 m-long, 35 mm-thick septum magnet and a 0.7 m-long electrostatic inflector (ESI) with maximum field strength of 0.5 T and 66.7 kV/cm, respectively, inject the 6 MeV/u ions with q/A larger than 0.25 into the ring. Four fast bump magnets distort the beam orbit around the ESI during injection. Bump magnets are made of 0.35 mm-thick laminated silicon steel and powered by thyristor switched condenser discharging circuit.

SYNCHROTRON MAGNET

A sector type dipole magnet[19] is used to suppress a change of vertical betatron function with tune around the operation point. An H-gap design of the dipole with saddle shape coil configuration is adopted to obtain a wide region of uniform field. The dipole magnet has demountable pole end pieces made of glued stack of lamination silicon steel at both ends. This enables the shim control of the magnetic length (Bl-product) of each dipole magnet by adding or omitting thin sheets between the pole and the pole end piece at four ends of the magnets. Fig. 7 shows a photograph of the dipole magnet. Specifications of the dipole magnet are summarized in Table 8.

To make a magnet yoke with a radius of curvature equal to bending radius and with sector edges, 12 types of lamination sheets with different sizes are made as liners from full size stamped lamination sheets. These liners and full size lamination sheets are stacked on a curved bed to form a sector yoke. The 100 mm-long outer parts at both ends of the yoke are glued respectively and have a rectangular shape. So the dipole magnet has actually a small edge angle of 0.88°.

The upper coil and the lower coil are not connected electrically inside a magnet, but are connected separately from magnet to magnet in cross-over configuration in the ring. Magnet yokes are also connected from magnet to magnet and finally to the neutral point of the magnet power supply. This configuration forms an electrical network and is expected to suppress current spikes associated with thyristor switching of the power supply.

To measure the magnetic field distribution of the dipole magnet, a computer controlled 4 m-long curved table was used to map the whole area of the magnetic field with a Hall probe. Measurements on field excitation and radial field distribution showed that the stacking procedure was adequate and that the punched pole cross section shape satisfied the specification on the field distribution.

To adjust the magnetic field lengths of 12 dipole magnets in each ring, two sets of measuring coil system with equal geometry were fabricated. Each coil system consists of 4 sets of 1250 mm-long single search coils, which approximate the reference orbit in the magnet. These 8 single search coils were calibrated to within $\pm 3 \times 10^{-5}$. Each dipole magnet to be installed in the ring was excited in series with reference magnet from 0.1 T up to 1.0 T and the difference of the outputs of the two coil system in the magnets was measured. The shim control of the magnetic length (Bl product) was performed with precision $\pm 0.8 \times 10^{-4}$ to each series magnet by adding or omitting laminated sheets between the poles and the pole end pieces at both ends. At 1.5 T the Bl products of the ring dipole magnets have a larger deviation of $\pm 3.5 \times 10^{-4}$ due to saturation of the magnet yoke. The positions of dipole magnets in each ring were determined by a suitable pairing such that the 4th harmonic component of the error distribution of Bl products of the dipole magnets in the ring would be reduced at 1.5 T.

The quadrupole magnet with saddle shape coils has a yoke with vertical length larger than horizontal length. This facilitates a design of the extraction beam channel while keeping the magnetic field in the yoke reasonably low at full excitation. The quadrupole magnet also has a glued demountable pole end pieces at both ends. Two upper coils and the two lower coils of the quadrupole magnet are also connected electrically from magnet to magnet in cross-over

configuration. Figure 8 shows a photograph of the quadrupole magnet with field measurement device. Specifications of the quadrupole magnet are also summarized in Table 8.

Field measurement with short twin coil system showed that the punched pole cross section shape satisfied the specification on the field distribution. Measurement with long twin coil system was performed to determine the end cut shape of the pole end pieces.

Sextupole magnet is 100 mm-long and its aperture is 252 mm in diameter. Maximum field strength is 45 T/m^2.

Table 8 Specifications for the dipole and the quadrupole.

Dipole magnet	
Number/ring	12+1††
Required field	1.5 T
Magnet length	3.4 m
Magnet type	H-gap sector type
Good field region Hor / Ver	210 / 50 mm
Vertical gap	66 mm
Field flatness $\Delta B/B$	$\pm 2 \times 10^{-4}$
Bending angle	30 degrees
Field rise	2 T/s
Magnet yoke size	1170^{w} x 680^{h} x 3400^{l} mm
Number of coil-turns	40
Current	2070 A
Coil resistance	18.5 mΩ
Coil inductance	51.6 mH
Magnet weight	24 ton
Quadrupole magnet	
Number/ring	24
Maximum field strength	7.4 T/m
Aperture diameter	192 mm
Magnet length	400 mm
Good field region Hor/Ver	244 / 56 mm
Gradient flatness $\Delta G/G$	$\pm 2 \times 10^{-3}$
Magnet yoke size	900^{w} x 980^{h} x 400^{l} mm
Number of coil-turns/pole	18
Current	1570 A
Coil resistance	9.6 mΩ
Coil inductance	9.0 mH
Magnet weight	3.2 ton
Magnet yoke material (Dipole and Quadrupole magnets)	laminated silicon steel Nippon steel corp. 50A600
Lamination thickness	0.5 mm

†† One dipole is used for on-line field measurements to generate a B-clock for rf acceleration.

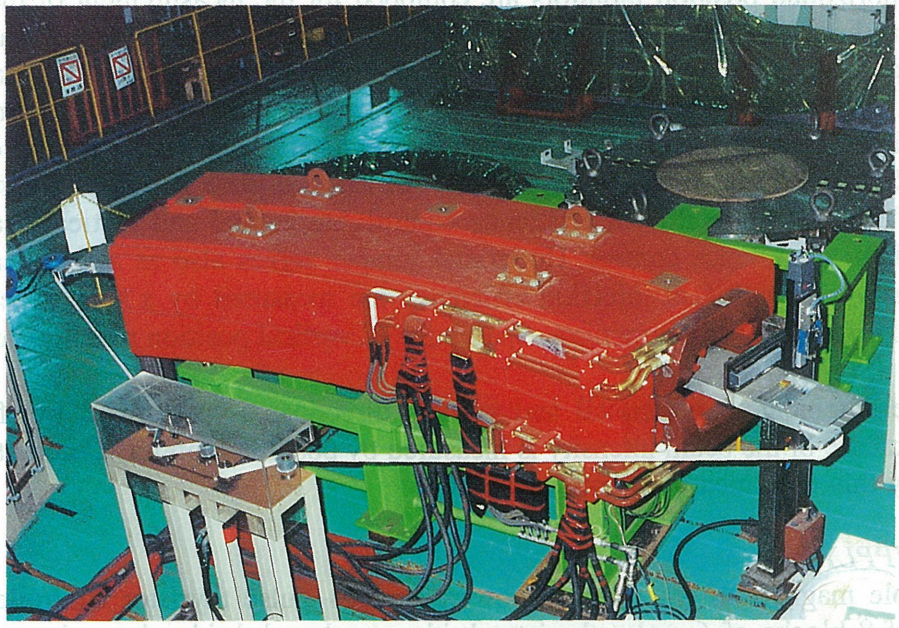

Fig. 7. Dipole magnet of the synchrotron with field measurement device.

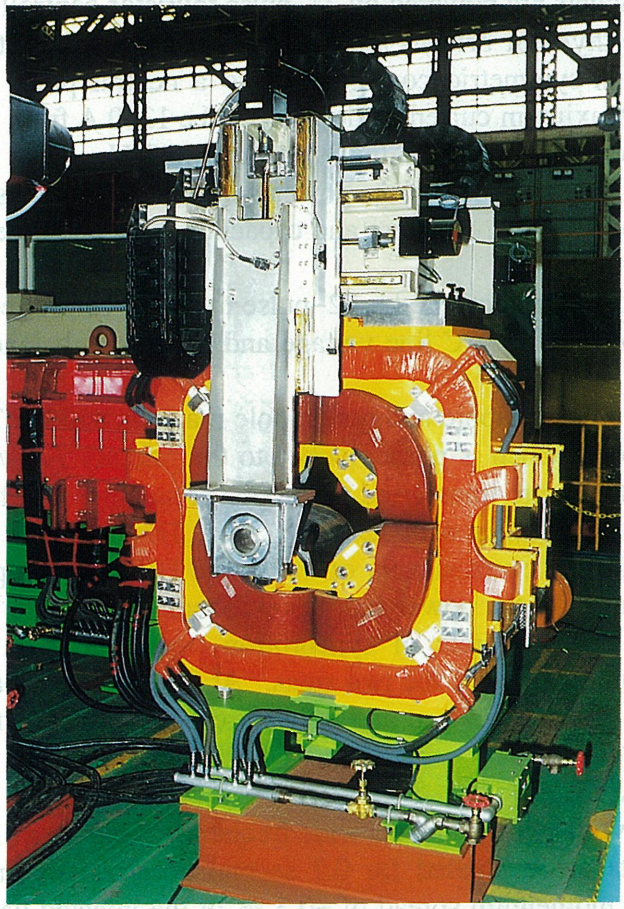

Fig. 8. Quadrupole magnet of the synchrotron during field measurement.

BEAM MONITOR

Twelve horizontal position monitors are equipped for the measurement of the horizontal closed orbit distortion[20]. They are installed in the horizontal steering magnets. Two horizontal position monitors are located at both ends of the accelerating cavity for rf acceleration control[21]. They are also used as a phase monitor. Two profile grid monitors are installed for first turn control. A Faraday cup is located one turn after the electrostatic inflector (ESI) for first turn efficiency control. An isolated plate is placed behind a septum electrode of the ESI for multiturn efficiency control. Horizontal and vertical beam scrapers are installed for emmitance control. Horizontal scraper serves also as a ring beam damper. Beam intensity and multiturn injection efficiency are measured by a sum of left and right signals of a horizontal position monitor. Spaces for 12 vertical position monitors and a current transformer are reserved.

Tune measurement in horizontal and vertical directions is performed by rf knock out method. Decrease of the beam intensity is measured by position monitor. Chromaticity is also measured by this tune measurement system[20].

POWER SUPPLY[22]

The dipole magnets of the ring are powered by 24-pulse thyristor controlled rectifiers consisting of 8 blocks of 6-pulse thyristor bridges and each bridge has a bypass thyristor. These blocks are assembled in a symmetric configuration to a neutral point of the power supply and are operated in converter-inverter mode at flat top and injection. Maximum current is 2260 A. Maximum output voltage is 2270 V.

The quadrupole magnets are powered by 24-pulse thyristor controlled rectifiers consisting of 4 blocks of 6-pulse thyristor bridges and each bridge has a bypass thyristor. These blocks are also assembled in a symmetric configuration to a neutral point and are operated in a converter mode only. Maximum current is designed to be 1360 A from the preliminary results of the field measurement. Maximum output voltage is 343 V.

Each passive filter of the synchrotron power supplies is composed of a normal mode reactor, a common mode reactor, resistors and capacitor. It is also assembled in a symmetric configuration to a neutral point.

The reactive power is compensated by 12-pulse thyristor controlled reactors (TCR). The TCR also stabilizes the primary AC line voltage and reduces imbalance of primary AC line voltage.

All power supplies for the dipole and quadrupole magnets and the TCR are controlled by a common 1200 Hz clock which is phase-locked to the primary AC voltage. Digital data of current and voltage patterns are transferred to the power supplies and to the TCR from VME fast digital output (FDO) modules with 1200 Hz clock. This 1200 Hz clock also serves as a timing clock to generate the event signals of the whole HIMAC complex.

A feed-forward control of the power supplies will realize a precise tracking of the current pattern outputs. The repetition rate of synchrotron operation is in a range 0.3-1.5 Hz depending on extraction energies of the two rings. At 0.5 Hz, a flat base time, a rising time and a flat top time are 0.1 sec, 0.7 sec and 0.5 sec respectively with field rise of 2 T/sec.

RF ACCELERATING SYSTEM

The rf accelerating voltage must have a wide frequency range from 1 MHz to 8 MHz. The rf voltage requirements are evaluated for 0.7 second acceleration time up to 600 MeV/u (dB/dt=2 T/sec) with a momentum spread of ±0.3 % of the injected beam from the linac and a filling factor of 0.8. The total energy gain per charge is about 1.7 kV and the peak cavity voltage is 10 kV for ions with q/A=0.5 and 11 kV for Ar^{18+}.

The rf cavity has a single gap structure which consists of a pair of ferrite loaded quarter-wave coaxial resonators coupled by a figure-of-eight configuration of bias windings. Figure 9 shows the rf cavity. Specifications of the rf cavity is shown in Table 9. The first cavity was fabricated and tested in order to confirm the performance[23]. Recently the cavity was powered at 9 kV successfully for the entire frequency range. Test with higher voltage is scheduled.

The operation patterns of rf frequency, voltage and ferrite bias current are generated by pattern memory modules. Event signals synchronized to the 1200 Hz control clock initiate capture, acceleration, flat-top and reset processes. Capture and flat-top event signals start the memory read-out by 10 kHz T-clock. The acceleration event signal starts the memory read-out by B-clock (field-clock). The B-clock generates a pulse at every 0.2 G change and has two components; up and down signals to respond the ripples of the dipole magnet field. Address of the memory modules goes up and down by the up and down signals of the B-clock.

Fine tuning by beam feedback control is performed by signals from beam-position and beam-phase monitors[21]. The beam monitors are located at both ends of the rf cavity. The beam monitor signals are buffered by FET amplifiers with 100 kΩ input impedance and are summed to reduce the rf noise. White noise level of the amplifier at input is 2 $nV_{rms}/\sqrt{Hz}$. The beam monitor signals and the rf cavity voltage are processed by heterodyne frequency converters to reduce a white noise component and to get a high fidelity over wide frequency range. Double conversion with 50 MHz and 455 kHz intermediate frequencies (IF) are processed. Beam displacement and beam phase signals are obtained from 455 kHz IF signals by amplitude-to-phase converter and synchronous phase detector, respectively. The feedback beam signals are digitized with sampling rate of 500 kHz to obtain a fast response. The fine tuning feedback signals and the rf pattern data from the memory module are digitally summed and are transferred to a digital synthesizer with 51 – 58 MHz output frequency. The digital synthesizer was adopted as a main rf signal source to reduce a residual FM noise and to obtain an accurate frequency setting. It is then converted to 1 – 8 MHz rf frequency by heterodyne converter and transferred to the rf power amplifier of the cavity[24,25].

In order to confirm the performance of the rf control system, it was installed in the TARN II rf accelerating system at Institute for Nuclear Study, University of Tokyo. He^{2+} ion beam with intensity as low as $8x10^6$ ppp was successfully accelerated from 10 MeV/u to 160 MeV/u[26].

EXTRACTION

A third-integer resonant extraction scheme is used to slowly extract the beam from the ring. Series of four slow bump magnets deform the closed orbit around electrostatic deflector (ESD) and control the position of the separatrix in phase space dynamically during extraction. Two pairs of sextupole magnets and a pair of tune control quadrupole magnets together with the main quadrupole magnets control the size of the separatrix. Two successive 1.3 m-long, 70 kV/cm ESDs and two magnetic septa eject the beam outside the ring. Septum electrodes of the ESDs are made of thin tungsten plate instead of wires. This choice was done to avoid the disturbance of the injected beam orbit by the leakage electric field. Thickness of the septum electrode of the upstream ESD is 0.3 mm. The high voltage of the upstream ESD is varied during extraction to improve the emittance of the extracted beam. Two magnetic septa are 1.2 and 1.18 m-long with field strength of 0.58 and 1.58 T. The magnets are outside vacuum duct and are operated at 100 % duty factor.

Table 9 Specifications of the HIMAC rf cavity.

A pair of ferrite loaded quarter-wave coaxial resonators.

Frequency range	1 – 8 MHz
Harmonic Number	4
Peak rf voltage	11 kV
Total length	2.77 m
Ferrite material	TDK SY6
Ferrite ring dimension	ϕ500 x ϕ320 x 25 mm^3
Number of ferrite rings	24 x 2
Bias current	10 – 900 A
Number of bias windings	4
Vacuum duct diameter	190 mm
Cooling water flow	60 l/min
rf power amplifier tetrode	Eimac 4CW100000E
Output power	30 kW

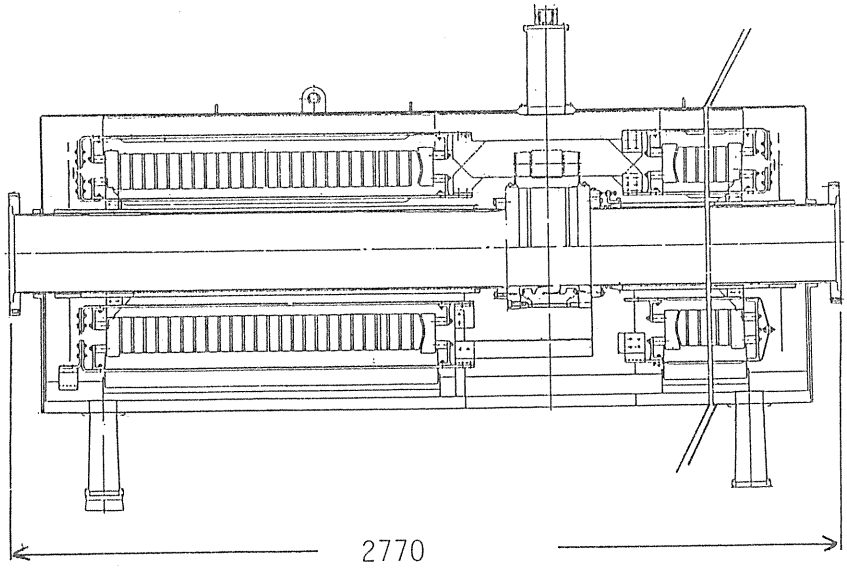

Fig. 9. rf cavity.

EXTRACTION BEAM TRANSPORT SYSTEM

Extraction beam transport system[18] transports the slowly extracted beam from each ring to high energy beam transport system. Multiwire beam profile monitors are installed to control the position of the extracted beam centroid. A plastic scintillation counter is installed to monitor and correct the beam spill ripple.

A fast beam shutter is installed and is controlled by the global interlock system of the HIMAC. The extracted beam is stopped here and the beam tuning is performed before delivering to the downstream high energy beam transport system. The shutter is also used for the accurate dose control in clinical treatment and for security in the treatment rooms.

VACUUM SYSTEM

In order to realize a vacuum pressure around $5x10^{-9}$ Torr, vacuum ducts, vacuum chambers and all components in the vacuum of the synchrotron ring are bakable at 200°C. Turbo molecular pumps, sputter ion pumps and titanium getter pumps are distributed in the ring to realize the vacuum.

Vacuum ducts in the dipole magnets are made of 0.3 mm-thick SUS316L and are reinforced by ribs to suppress the eddy current due to the ramping magnetic field. The vacuum ducts for the dipole magnets are directly heated by DC current flowing in the duct wall in baking. Other vacuum ducts and vacuum chambers are heated by mineral insulated heaters attached on their surface walls in baking.

CONTROL SYSTEM[27]

A DEC VAX 4000/300 computer serves as a man machine interface coordinator through operator console and as a file server of the synchrotron operation. This main computer is connected to central computer through an ethernet by which the synchrotron subsystem communicates with other subsystems.

Real time control of the power supplies is performed by several VME controllers under PDOS real time OS. The controllers are connected to the main computer through another ethernet. The output current and voltage of the DC power supplies are directed and monitored by digital I/O units. Besides usual DI and DO units for DC power supplies, fast DI and DO units are developed to control power supplies with pattern outputs. Each of these FDO units has a dual memory which enables a quick change of the patterns. Beam monitors are also controlled by the VME controllers.

Warning signal monitoring and on/off control of the power supplies are performed by sequence controller (PLC) to ensure a reliable operation against noises under accelerator environment.

The above mentioned FDO's are also used to generate timing signals because of the repetitive nature of the synchrotron operation. FDO's deliver the event signals such as injection, capture, acceleration, monitor timing and so on to the whole HIMAC complex in synchronous to the 1200 Hz clock from the synchrotron magnet power supply system.
The rf system is controlled by a dedicated small computer for the independent check of the operation. The rf computer is also connected to the main computer via an ethernet within a synchrotron sub-system.

HIGH ENERGY BEAM TRANSPORT SYSTEM

Requirements for the high energy beam transport (HEBT) system[28,29] are 1) to deliver horizontal and vertical beams, 2) to realize simultaneous irradiation by horizontal and vertical beams at different energies for the same patient or two different patients, 3) to switch beams from one treatment room to another in a very short time.

The HEBT system consists of a horizontal and a vertical beam line as shown in Fig. 10. The horizontal beam line is designed to transport the beam from the lower ring. The beams up to 800 MeV/u are provided to two treatment rooms (B,C) and a physics-general experiment room, and the beams up to 600MeV/u to a secondary beam experiment room. On the other hand, the vertical beam line is designed to guide the beam from the upper ring and that from the lower one through a junction beam line. It can transport the beams up to 600 MeV/u to two treatment rooms (A,B) and a biological experiment room. It is possible for the same patient to be irradiated simultaneously by horizontal and vertical beams in the treatment room B. Further, a switching magnet at the junction of the line is of a laminated structure. Therefore, the beams from the upper ring and the lower one can be transported alternately to the same target.

For achieving a required dose uniformity (±2%) even the case of a broad beam (max. dia. of 220 mm) which is obtained by using scanner magnets and scatterer, the beam optics is designed such that the beam at each isocenter satisfies a doubly achromatic condition and is within the size of 10 mm. A typical calculation result is shown in Fig. 11. Besides, this set of beam optics keeps the design acceptance of 10 πmm·mrad when the pole gap of all bending magnets are downsized to 60 mm for cost reduction. In addition, the beam should be switched within 5 minutes from one course to the other by only adjusting the current of the switching magnet in order to obtain an efficient beam use for a treatment. The reproducibility of the beam position is required to be within ±2.5mm after beam switching. To satisfy the requirements, an excitation procedure of the magnet will be programmed for an initialization and setting the current, and its magnetic field will be precisely monitored by NMR. A residual field of the switching magnet will be also compensated by using a small current source.

Beam profile monitors and steering magnets are assigned to reduce the beam centroid displacement within the size of 5 mm at a standard deviation. The beam profile monitor, which is a multiwire proportional chamber, was tested by using a proton beam of 70 MeV at NIRS and worked well in the intensity range corresponding to helium beams of 800 MeV/u at $1.4\text{x}10^{6}$ ~ $1.4\text{x}10^{11}$pps.[30]

The secondary beam line will be prepared for the study of diagnostic and therapeutic applications of a radioactive beam, which also separate the designed secondary beam from the primary and other projectile fragments. In the secondary beam line, the momentum spread can be suppressed within ±0.2% by using a wedge degrader and analyzer magnets. By using the radioactive beam, one can measure precisely the stopping point of the beam in a patient's body, and the treatment will be performed by using stable heavy ion beams with the same range as the radioactive beam. The vertical beam line from the upper ring is also applicable for the same purposes. The produced radioactive beam is analyzed by four bending magnets and a slit, and is transported to the treatment room A or B.

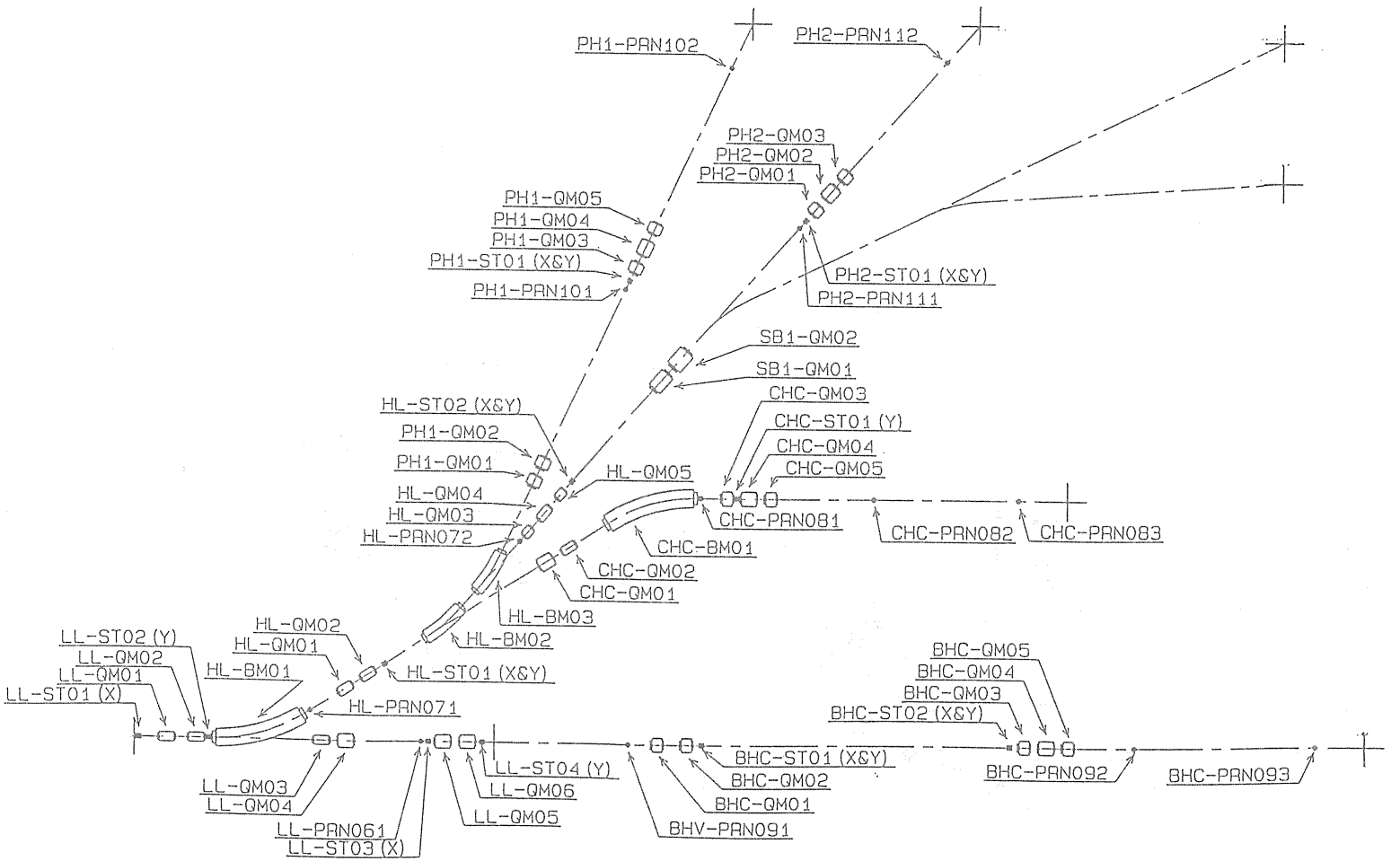

Fig. 10(a). A plan view of the horizontal beam lines.
BM : Bending magnet, QM : Quadrupole magnet,
ST : Steering magnet, PRN : Profile monitor

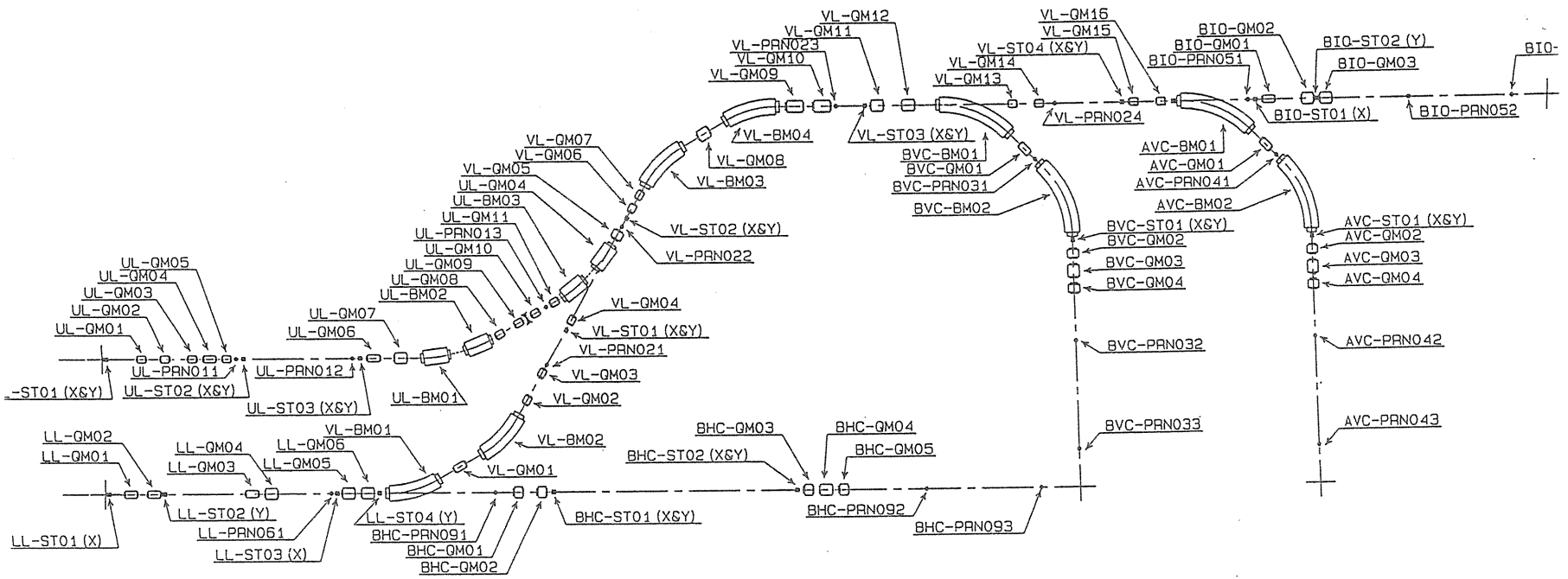

Fig. 10(b). A side view of the vertical beam lines.

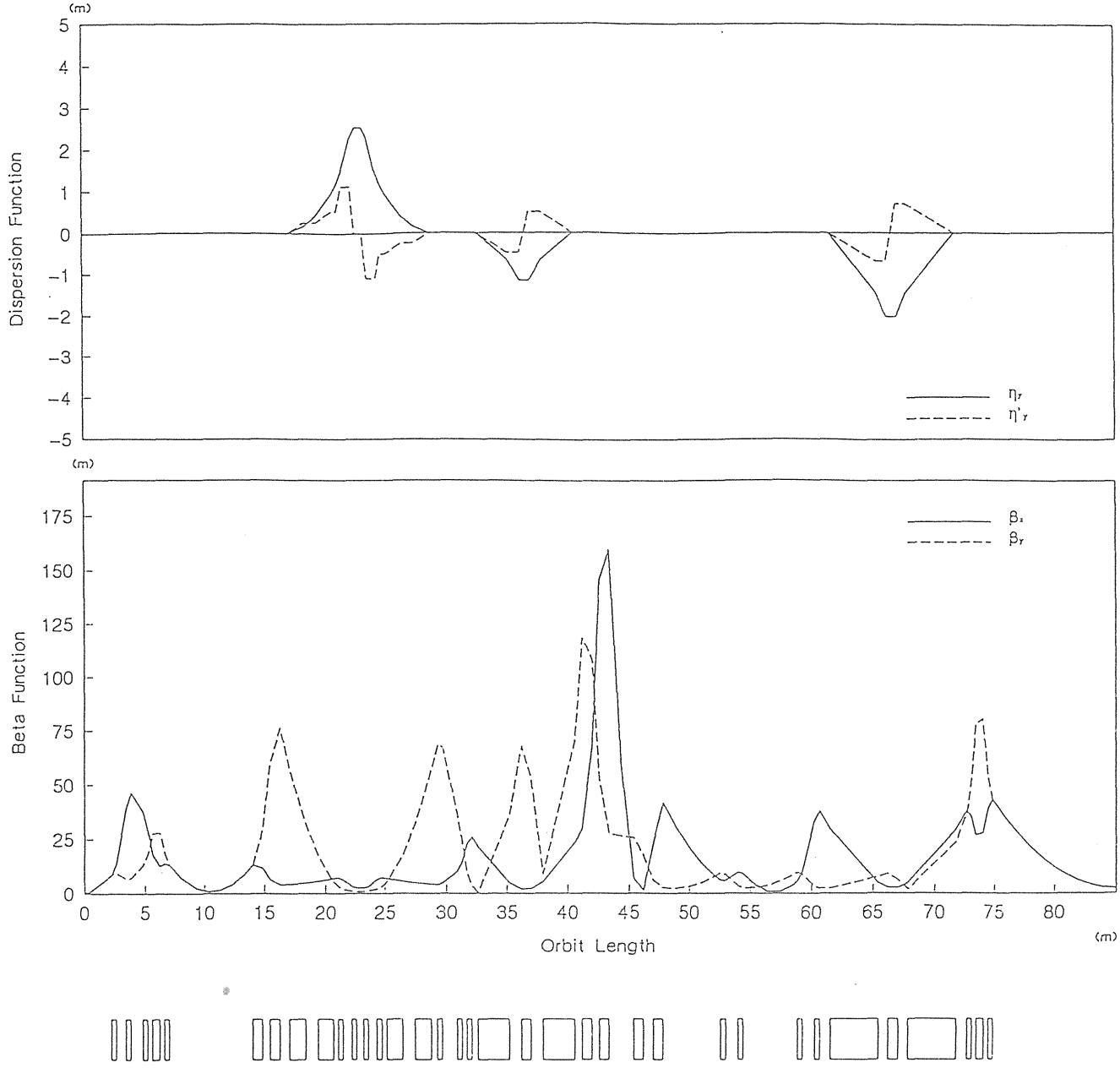

Fig. 11. Dispersion function (η_y, η'_y) and beta function (β_x, β_y) of the vertical beam line to the isocenter of the treatment room A.

TREATMENT SYSTEM

There are three clinical treatment rooms for patients. The room A has a vertical, the room C has a horizontal and the room B has both vertical and horizontal beam courses, which have a common isocenter for the patient. The accelerators and the treatment rooms are connected by a high-energy beam transport system. By switching rapidly the beam transport lines from two rings, different beams can be delivered to each room. This will greatly increase the efficiency of the therapeutic utilization of the beam. The HIMAC treatment facility [5,31,32] consists of a beam delivery and irradiation system, a patient's positioning system[33], and a treatment planning system[34].

BEAM DELIVERY AND IRRADIATION

To make uniform irradiation fields within ±2% of accuracy, we have chosen a beam wobbling method[35]. In the wobbler method developed at LBL, wobbled beams of several radii were superposed to make large uniform field. In our case, uniform field is made by wobbling a scattered beam with one radius of rotation[36]. Disturbance of the dose uniformity on the target volume due to the movements during the irradiation is expected to be much smaller than the linear scanning method developed at LBL[37] or GSI[38].

The layout of the beam delivery system in the horizontal beam course is shown in Fig. 12. The beam delivery system comprises a pair of scanning magnets (wobbler magnets), a beam scatterer, a ridge filter, a range shifter, a block collimator, a multileaf collimator and several beam monitoring devices. The irradiation systems for horizontal and vertical beams have exactly the same components.

The beam delivery system is laid across the neutron shutter which is embedded at the wall separating the treatment room from the area of the upstream high-energy beam transport line. It is supposed that while the beam is stopped at the beam shutter just before the neutron shutter for beam tuning, medical staff can engage in the various works such as the patient positioning in the treatment room. In order to fulfil the condition that the neutron produced at the beam shutter is sufficiently attenuated in the treatment room, the size of the neutron shutter becomes fairly large. For the fast neutron, the path length to block the neutron parallel to the beam line should be equivalent to the wall thickness of 2.5 m concrete which corresponds to 90 cm of iron, and in case of oblique direction of more than 30 degrees to the beam line, the shielded path of the projected length to the beam line is set to be more than 70 cm of iron. For blocking of the thermal neutron, the constraint is set that the inevitable clearance between different parts should be within 5 mm. Basic mechanism is that a slider of the rectangular parallelepiped block made of stainless steel having a typical weight of 1.5 tons is moved perpendicular to the beam direction in the evacuated chamber. The movement of the slider is carried out using the speed-controlled driving motor.

One of the two beam profile monitors is located upstream of the neutron shutter and the other before the block collimator. These are multiwire proportional counters used to see the beam profile at the tuning time of the beam transport.

A pair of the scanning magnets are orthogonal bending magnets and they are used in association with the beam scatterer to form a uniform field dose in the lateral distribution at the isocenter. The electric power supplies for the scanning magnets feed the sinusoidal current with the frequency of 57 Hz, which is selected to avoid the non-uniformity due to pickup of the noise synchronized with line frequency. With the phase difference of 90 degrees between two magnets, the wobbler magnets give rise to the circular rotation of the beam spot at the position of isocenter. The multiple scattering by the scattering foil causes

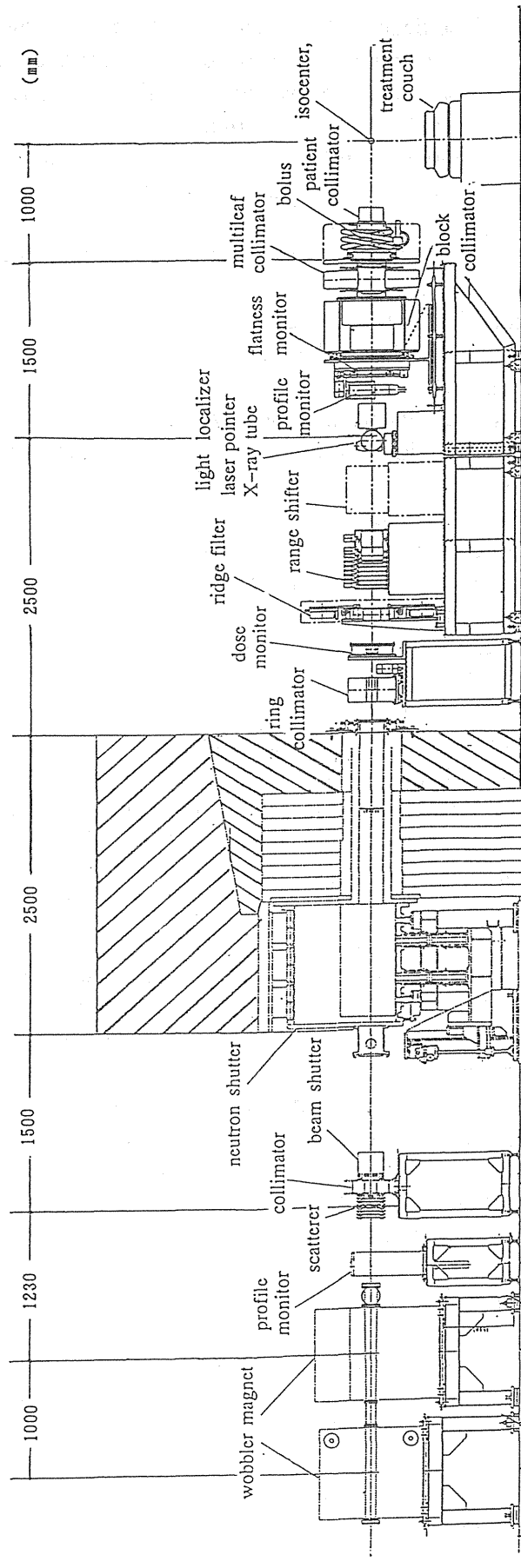

Fig. 12. Layout of the beam delivery system.

the Gaussian distribution of the beam in the transverse plane. The thickness of the foil ranges from 0.1 to 12.8 mm (Pb equivalent) and 8 different foils are attached. The convolution of circular movement of this broadened spot by means of the magnetic fields produces the flat distribution within ± 2 % inside the certain diameter at the position of the irradiation. Considering the distance of about 10 m between the magnets and the isocenter, the required maximum magnetic field is 2 kG and the peak current of the coils is approximately 1000 A. The positions of the magnets, the scatterer and isocenter, and their associated conditions are determined from the beam optics and simulation of the beam tracking including the effect of the particle flight in the air.

The ridge filter spreads the narrow Bragg peak according to the thickness of the tumor. We intend to use the so-called bar-ridge filter. This is a range modulator that in the transverse plane, about ten metallic bars are set in a row, and each bar has the cross section of triangle shape meaning the varying thickness with fine steps along the beam path. The height and their ratio of the width of the fine steps are determined by the requirement considering the thickness of the tumor. Seven different filters made of Al or Cu can be set in the large circular frame of rotation.

The range shifter is a device which uses absorbers to fine tune the ion range to conform the depth of the tumor. They are nothing but energy degraders of different thicknesses. Nine absorbers, from 0.5 to 128 mm in thickness, made of lucite are prepared and these are driven in and out on the beam path with electric driving system.

The Al block collimator is composed of movable 4 slit-leaves of 20 cm in thickness which roughly cut most of the irrelevant portion of the spread beam.

The multileaf collimator is a field-shaping device which tailors the beam according to the perpendicular cross section of the tumor. Very thin metal leaves are stacked close to each other. They are made of Zn-coated iron. The maximum opening between two opposite leaves is 22 cm. Each leaf has a 16 cm stroke. The irradiation area is 15 x 22 cm^2 at maximum. The height of each leaf is 6.25 mm. The number of leaves is 23 at each side of the aperture. The thickness of the leaf along the beam direction is 14 cm. The clearance between neighboring leaves is within 0.25 mm. Each leaf has two step stairs of 0.6 mm difference of the height along the beam path to block the beam passing straight through the gap between neighboring leaves. The leakage of the beam including the contribution from the fragment under certain assumption is simulated in the calculation and that is expected well below the treatment standard[39]. The positioning of the leaves is performed with the stepping motors under the computer control. The block collimator and the multileaf collimator are bound together and whole system can be rotated 90 degrees around the central ray of the beam. Therefore, the leaves can be operated at the suitable angles depending on the shape of the tumor of the patient. In order to satisfy the requirement that the collimator can be placed as close to the patient as possible, on the other hand a certain vacant area of the cross section must be assured at the time of X-ray irradiation, these collimator system are designed to displace the position along the beam line. The distance from the isocenter can be varied from 50 cm to 100 cm in the horizontal beam course. Whole area perpendicular to the beam of these instruments is compactly contained within 85 cm in diameter.

In order to measure and record the irradiation dose, the principal and subordinate ionization chambers are placed separately as dose monitors. All the associated modules and electronics are set independently. These are designed to protect against an overdose of irradiation in case of either counter disabled.

The flatness monitor comprises 25 segmented sensitive parts in an ionization chamber. These are to be monitored continuously to keep the beam intensity distribution uniform in the irradiated area. All of these devices are to be operated under the computer control and the

signals are monitored and illustrated with a pulse to pulse basis on the graphic panel.

The beam compensator (bolus) and the patient collimator, in certain cases, are to be set just in front of a patient.

All of these apparatus are controlled and operated via treatment control computer (HP 9000/380). 3 computers are assigned each to 3 different rooms.

These computers are supervised by an irradiation managing computer (HP 9000/380) which links the irradiation or treatment system to the HIMAC central control system.

While the design of the facility is principally aimed at clinical purposes, safety and protection against accidental irradiation of patients, or technical and medical staff are one of the important items. Anticipating as many probable incidents as possible, a careful interlock system is built into the safeguards against overdoses, problems with instruments, change of beam intensity and change in the condition or position of the patient. Suspension of irradiation, quick restart, stop of irradiation ; these are linked with operation of beam shutter and neutron shutter either by automatic or manual operation. They are synthesized in a global interlock system which is driven with threefold safeguards through hardware and software.

PATIENT POSITIONING

The patient positioning system consists of laser pointers, a light localizer, X-ray tubes, image intensifier tubes, a treatment couch, patient immobilization aids and an X-ray CT. The laser pointer is an indicator of the beam center for heavy-ion treatment. Due to the fact that each room has different beam course, in the room A and the room B 3 laser pointers are utilized and 5 of those are set in the room C, including one pointer on the way of beam path in each course which is displaced at the time of beam irradiation. The light localizer is the projector of the parallel light and placed on the beam line near the position of the X-ray tube. It is used to check the setting of the shape of the multileaf collimator projected on the patient.

X-ray tubes and image intensifier tubes with TV are to be set in two perpendicular directions, one of which is a beam's eye view and the other is from its perpendicular direction. In the room C, due to capability of the two different positions of the patient; the lying and the sitting on the couch, the 3 sets of the X-ray tube and the imaging intensifier are placed. They are used for verification of the beam direction and the target volume position with use of certain numbers of anatomical landmarks. By comparing the positions of landmarks in the X-ray image at the time of patient positioning on the couch and those on the reference image from the digitally reconstructed radiographs which is generated at the time of treatment planning, the calculation using the coordinates of landmarks gives the amounts of the required displacement of the patient's couch.

The movement of the treatment couch will be controlled by the patient positioning computer (HP 9000/730) linked to image verification devices. The displacements in horizontal plane and adjustment of the height, and rotation in the horizontal plane and movements of rolling and pitching within ± 10 degrees can be performed in all the 3 patient couches.

We are going to install the X-ray CT in the treatment room B. This is to verify the setting position more precisely with respect to the field size and depth at each slice of the patient. Along the guide rail on the rotating table on the floor, the patient couch can be displaced and inserted in the gantry of the X-ray CT installation assuring the reproducibility of the position.

A modifier, such as a compensator and a patient collimator, will be designed and made for individual patients with the help of a treatment planning computer and a numerically controlled machine. The overall layout in the room B is illustrated in Fig. 13.

Fig. 13. Layout of the room B.

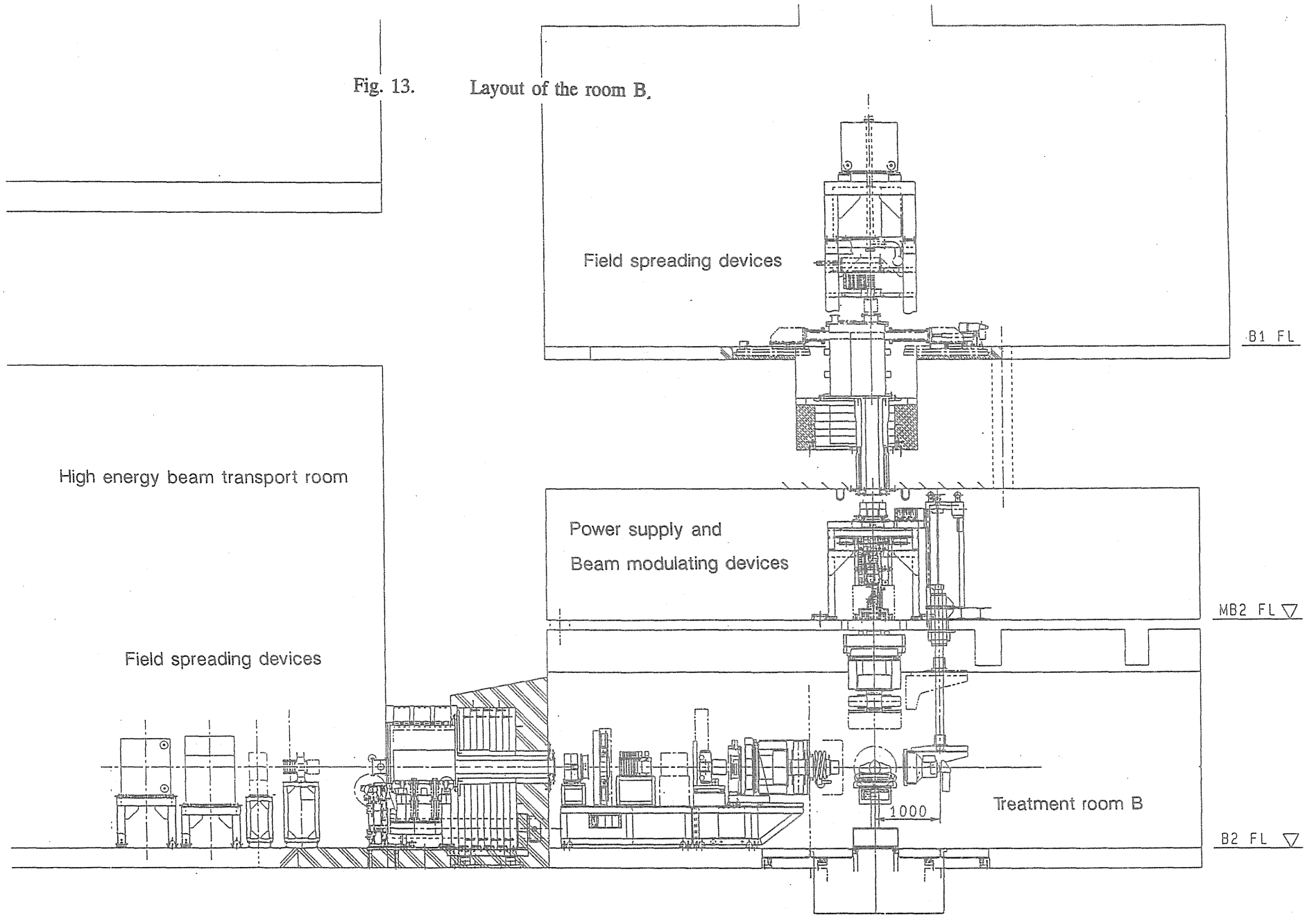

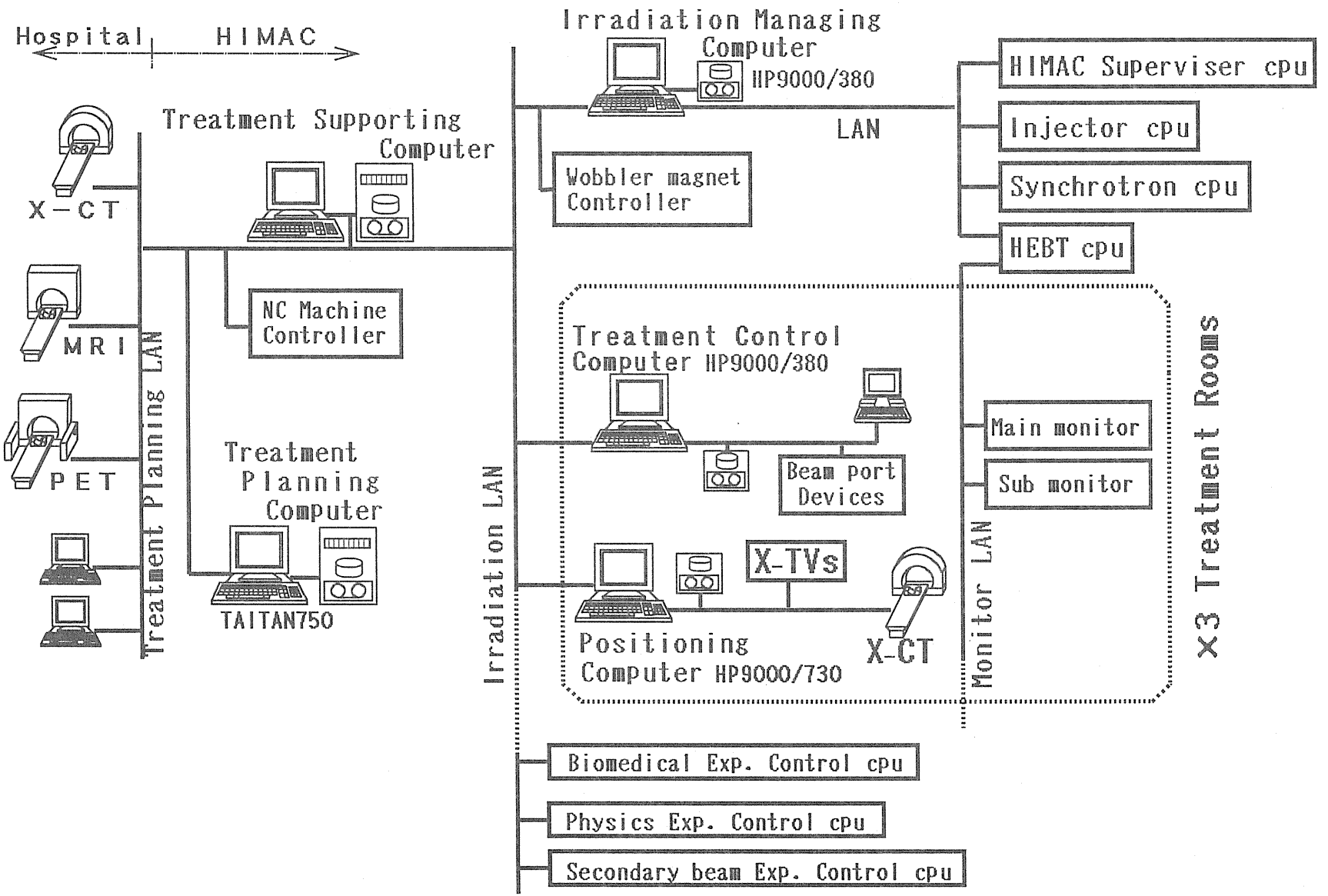

Fig. 14. Network system in the treatment control system.

TREATMENT PLANNING

Three dimensional treatment planning system is developed on the treatment planning computer; a super graphics workstation (TITAN 750). Treatment planning consists of the following procedures: 1) defining target volume and critical organs by interactive contouring on X-ray CT, MRI or PET images, 2) determination of directions and shapes of irradiation fields using beam's eye view graphics, 3) calculation and display of three dimensional dose distributions, taking account of inhomogeneous electron density and biological response factors in the body. 4) designing collimators and compensators, 5) generating digitally reconstructed radiographs which are used for patient positioning. In addition, the treatment supporting computer converts the planning data to the treatment control data, which consist of beam parameters, port data and treatment couch parameters. A schematic view of the treatment control networks under design is shown in Fig. 14. In future, additional investigations, such as radioactive beam implantation, and heavy-ion imaging will be in due course performed for the precise heavy-ion treatment.

THREE DIMENSIONAL CONFORMATION THERAPY

In order to utilize the excellence of the dose localization of the beam to the utmost, the three-dimensional conformed irradiation is designed in the irradiation system. The three-dimensional irradiation system for proton raiotherapy using a broad beam has been proposed ten years ago[40]. In the three-dimensional irradiation of heavy ions, the dose uniformity in the target will be disturbed because of the complexity of overlapping caused by the fragmentation tail. However, in case of heavy ions lighter than carbon, the disturbance will be disregarded clinically. A sophisticated method using a beam scanning[37,41,42] needs more technical developements, such as completing the irradiation in a short time, to avoid dose disturbances due to the target movement. Therefore we adopted the above method using a broad beam in the three-dimensional irradiation.

Our present scheme is as follows. Laterally, a uniformly broadened field is obtained by the wobbler magnets and scatterer. Along the depth of the tumor, the target volume is divided to many slices and the ridge filter is set to spread out the Bragg peak to corresponding thickness for one slice. When each slice is irradiated step by step in order, the depth of the range is changed by the variable range shifter which is composed of two wedge shifters. At the same time, the lateral shape of the field is changed by the movement of multileaf collimator which tailors the cross section of the target volume for each slice.

The timing of these movements are controlled by the signal from dose monitor. Every time the monitor count reaches the preset count at each slice which is determined from the universal fraction curve associated with spread-out Bragg peak, the field shape and depth are adjusted for next slice. The range is swept several times within target thickness to average a dose at the slice, since the position of the slice may be disturbed by the movement of the target. Typically the number of sweeps are repeated 5-10 times back and forth over the target area. The irradiation time is a few minutes in case that the target thickness is 70 mm and the slice thickness is 5 mm. To realize this method, the deliberate planning of the dose distributions and the well controlled functioning of each mechanism are required.

OTHER EXPERIMENTAL AREA

The HIMAC facility includes not only clinical treatments, but also fundamental research works such as medical physics, radiation biology and radiation chemistry. A biological irradiation room is provided for small animals, for tissue-cultured cells and for the use of radioactive materials. This irradiation system is almost the same as the beam delivery system for the treatment rooms except for a multileaf collimator, which can easily simulate the

condition of the irradiation for the patients. A relatively large area of general irradiation room is provided for fundamental experiments in physics and other fields as well as radiation physics. A secondary beam irradiation room is prepared for the development of diagnostic and therapeutic applications of radioactive beams. In addition, one room is allocated for the experiment which will use the beams of 6 ~ 8 MeV/u from the injector linacs. Consequently, a variety of different kinds of irradiations or experiments is considered to be feasible in the facility.

CONTROL SYSTEM

HIMAC is roughly divided into the injector, the synchrotron, the high-energy beam delivery and the irradiation sub-systems. An overall control system for HIMAC consists of a supervisor control system and four control systems as mentioned above and they are connected via Ethernet. The supervisor system is used for the global control of the whole system of HIMAC. It is also connected by hardware and/or software to the other equipments in this facility such as a water-cooling system and a radiation safety system. On the other hand, the control system of each sub-system which consists of the main computer and some lower level computers is used for the control of individual devices. The main computer serves mainly as a man-machine interface and a file server. In the HIMAC system, operation parameters such as current values, current patterns, timing relations etc. are saved as parameter files in the main computer and referred as the reference data in the next operation of the identical condition. The main computer has to manage this database and carry out programmed start-up and shut-down sequences using these files.

Since the sub-systems are designed and manufactured by different companies, respectively, the computers and the interfaces of the different types are used among the sub-systems. Therefore the control system for each sub-system is designed in the following manner, that is, 1) hardware and software concerned with the man-machine interface must be standardized among all sub-systems, and 2) each system is operated rather independently by reducing the data to be transferred each other.

As hardware for the man-machine interface two 14-inch CRTs, two 20-inch CRTs, touch panels and rotary encoders are equipped at the operator console of each sub-system. Most operations are performed with them in the control room on the ground floor with common procedures to all sub-systems except for the irradiation system. The devices in the irradiation system are controlled at the consoles near the treatment rooms on the second basement. The synchrotron and the high energy beam delivery systems have two consoles, respectively, and this enables us to do operations independently for the upper and the lower lines.

The application software in all sub-systems is written mainly in C or FORTRAN. Furthermore programs of equivalent functions among the sub-systems are registered in the subroutine library of each sub-system with an identical name. Users can write application programs by calling these subroutines with device names, operation names and preset values even if they don't know the details of the interfaces between the computers and the devices.

A timing system is very important to synchronize the sub-systems because they are operated independently. Event signals are generated in the synchrotron system for this purpose. We can set the event signals at the arbitrary positions in the repetition cycle of the synchrotron. Each signal determines the timing of the specific event, for example, 'BEAM INJECTION', 'RF ON', 'ACCELERATION START', etc. and is delivered to the corresponding sub-system by hardware. The sub-system generates timing signals with a certain delay and width from this event signal and delivers to the devices.

The details of each control system are described in other articles[43,44,45].

ACKNOWLEDGMENTS

The cooperation of the manufacturing companies, Sumitomo Heavy Industries, Toshiba Corporation, Hitachi Ltd., and Mitsubishi Electric Co. were indispensable.

The authors would like to express our sincere gratitude to many physicists and engineers of numerous institutions, whose discussions and suggestions helped us in various phases of designing and construction of HIMAC. They include:
For the injector, Drs. T.Hattori(Tokyo Institute of Technology), Y.Miyazawa(RIKEN), S.Fu(STA fellow);
for the synchrotron, Drs. K.Endo(KEK), S.Matsumoto(Dokkyo Medical Univ.), H.Sato(KEK), K.Uchino(Tsukuba Univ.), T.Kato(KEK), Y.Irie(KEK), T.Kawakubo(KEK),T.Sueno(KEK), Y.Takada(Tsukuba Univ.), A.Mizobuchi(INS, Tokyo Univ., retired), T.Tanabe(INS,Tokyo Univ.), S.Watanabe(INS,Tokyo Univ.), A.Noda(ICR, Kyoto Univ.) and J.Staples(LBL, Univ. California);
and for the treatment system, L.Sihver(STA fellow).

The authors thank our colleagues in the institute for their invaluable support and help, especially Dr. H.Matsudaira, the Director General.

REFERENCES

[1] H.Tsunemoto, et.al., Int. J. Radiat. Oncol. Biol. Phys. 8 (1982) 2169.
[2] H.Tsunemoto, et.al., Radiat. Res. 104 (1985) S235.
[3] M.C.Pirraccello, et.al. Ed., LBL Report, LBL-11220 (1980)
[4] Y.Hirao, et.al., Proc. 2nd Euro. Accel. Conf., (1990) 280.
[5] K. Kawachi et al., J. Jpn. Soc. Ther. Radiol. Oncol. 1 (1989) 19-29.
[6] S.Yamada, et al., Proc. 7th Symp. Accel. Sci. Tech., RCNP, Osaka, Japan, (1989) 45.
[7] S.Yamada, et al., Proc. 1990 Linac Conf., Albuquerque, New Mexico, USA, (1990) 593.
[8] S.Yamada, et al., Proc. 8th Symp. Accel. Sci. Tech., RIKEN, Saitama, Japan, (1991) 28.
[9] K.Sawada, et al., *ibid.*, 158.
[10] Y.Sato, et al., J. of Appl. Phys. 69 (1991) 7933.
[11] Y.Sato, et al., Nucl. Instrum. Methods. A309 (1991) 348.
[12] Y.Sato, et al., Rev. Sci. Instrum. 63 (1992) 2904.
[13] A.Kitagawa, et al., Proc. 8th Symp. Accel. Sci. Tech. Saitama, Japan, (1991) 58.
[14] P.Sortatz, Rev. Sci. Instrum. 63 (1992) 2801.
[15] A.Itano et al., Proc. 7th Symp. Accel. Sci. Tech., RCNP, Osaka, Japan, (1989) 42.
[16] K.Sato et al., Proc. 8th Symp. Accel. Sci. Tech., RIKEN, Saitama, Japan, (1991) 31.
[17] K.Sato et al., Particle Accelerators 33 (1990) 147.
[18] K.Noda et al., Proc. 8th Symp. Accel. Sci. Tech., RIKEN, Saitama, Japan, (1991) 205.
[19] A.Itano et al., *ibid.*, 202.
[20] M.Sudou et al., *ibid.*, 320.
[21] M.Kanazawa et al., Proc. 7th Symp. Accel. Sci. Tech., RCNP, Osaka, Japan, (1989) 210.
[22] M.Kumada et al., Proc. 8th Symp. Accel. Sci. Tech., RIKEN, Saitama, Japan, (1991) 199.
[23] M.Kanazawa et al., *ibid.*, 161.
[24] M.Kanazawa et al., *ibid.*, 323.
[25] M.Kanazawa et al., Proc. EPAC92. and E.Takada et al., Proc. HEACC92.
[26] M.Kanazawa et al., Proc. 8th symp. Accel. Sci. Tech., RIKEN, Saitama, Japan, (1991) 326.
[27] E.Takada et al., *ibid.*, 353.
[28] H. Ogawa, et al., Proc. 7th Symp. Accel. Sci. Tech., RCNP, Osaka, Japan, (1989) 48.
[29] K. Noda, et al., Proc. 13th Int. Conf. Cyclo. Applicat., to be published.
[30] M. Torikoshi et al., Proc. 8th Symp. Accel. Sci. Tech., RIKEN, Saitama, Japan, (1991) 317.
[31] F. Soga et al., Radiat. Res. A Twentieth-Century Perspective (W. C. Dewey et al., Eds.) (1991) 641.
[32] F. Soga, Proc. NIRS Int. Workshop, NIRS, Chiba, Japan, (1991) 36.
[33] S.Minohara et al., J. Int. Fed. Med. Bio. Eng., 29 Supplement, (1991) 859.
[34] M. Endo et al., *ibid.*, 317.
[35] T.R.Renner and W.T.Chu, Medical Physics 14 (1987) 825.
[36] T.Kanai et al., Nucl. Instrum. Methods A302 (1991) 158.
[37] W.T.Chu et al., Proc. NIRS Int. Workshop, NIRS, Chiba, Japan, (1991) 110.
[38] Biophysics Group, GSI. GSI report 91-18.
[39] M. Sudou et al., J. Int. Fed. Med. Bio. Eng., 29 Supplement, (1991) 638.
[40] T.Kanai et al., Medical Physics 10 (1983) 344.
[41] Biophysics Group, GSI. GSI report 03-92 (1992) 16.
[42] E.Pedroni et al., Proc. NIRS Int. Workshop, NIRS, Chiba, Japan, (1991) 94.
[43] T. Kohno et al., Proc. 7th Symp. Accel. Sci. Tech., RCNP, Osaka, Japan, (1989) 246.

[44] T. Kohno et al., Proc. Int. Conf. Accelerator and Large Experimental Physics Control Systems, Tsukuba, Japan, (1991).
[45] S. Minohara et al., *ibid.*